Polarization Properties of Vertical-Cavity Surface-Emitting Lasers

J. Martin-Regalado, F. Prati, M. San Miguel, and N. B. Abraham, *Member, IEEE*

Abstract— Polarization-state selection, polarization-state dynamics, and polarization switching of a quantum-well vertical-cavity surface-emitting laser (VCSEL) for the lowest order transverse spatial mode of the laser is explored using a recently developed model that incorporates material birefringence, the saturable dispersion characteristic of semiconductor physics, and the sensitivity of the transitions in the material to the vector character of the electric field amplitude. Three features contribute to the observed linearly polarized states of emission: linear birefringence, linear gain or loss anisotropies, and an intermediate relaxation rate for imbalances in the populations of the magnetic sublevels. In the absence of either birefringence or saturable dispersion, the gain or loss anisotropies dictate stability for the linearly polarized mode with higher net gain; hence, switching is only possible if the relative strength of the net gain for the two modes is reversed. When birefringence and saturable dispersion are both present, there are possibilities of bistability, monostability, and dynamical instability, including switching by destabilization of the mode with the higher gain to loss ratio in favor of the weaker mode. We compare our analytical and numerical results with recent experimental results on bistability and switchings caused by changes in the injection current and changes in the intensity of an injected optical signal.

Index Terms—Laser stability, optical injection locking, polarization, polarization switching, quantum-well lasers, semiconductor lasers, vertical-cavity surface-emitting lasers.

I. INTRODUCTION

CONTROL of the polarization state of light emitted from vertical-cavity surface-emitting lasers (VCSEL's) is desired for a number of polarization-sensitive applications. The development of optical switches and bistable devices based on two orthogonal linearly polarized states requires such control. Unfortunately, from this point of view, emissions from VCSEL's can be quite complex in both the polarization state and transverse mode combination [1]–[9]. Their polarization stability is much less than that of conventional edge emitting lasers [9]. As the injection current is increased, there are often transitions from the lowest order transverse (Gaussian) mode to higher order transverse modes (or combinations of modes),

J. Martin-Regalado and M. San Miguel are with the Departament de Fisica, Universitat de les Illes Balears, and with the Instituto Mediterraneo de Estudios Avanzados, IMEDEA (CSIC-UIB), E-07071 Palma de Mallorca, Spain.

F. Prati was with the Dipartimento di Fisica, Universitá degli Studi di Milano, 20133 Milan, Italy. He is now with Il Facoltá di Scienze, Universitá deglie Studi di Milano, 22100 Como, Italy.

N. B. Abraham was with the Departament de Fisica, Universitat de les Illes Balears, E-07071 Palma de Mallorca, Spain. He is now with the Department of Physics, Bryn Mawr College, Bryn Mawr, PA 19010-2899 USA.

including complicated behaviors involving both pattern and polarization-state changes.

However, when the injection current is changed near the lasing threshold, variations in the polarization state of the fundamental Gaussian pattern can be distinguished [1]–[7]. In several experiments, it was found that laser emission on the fundamental spatial mode with linear polarization near threshold switched to the orthogonal linear polarization as the current was increased (e.g., see [5, Fig. 1] and [3, Fig. 2(c)] in the region of injection currents $I < 1.2 I_{\mathrm{th}}$). Polarization switching has also been biased or induced by an injected optical field of a particular polarization state [5]. It is an explanation for these phenomena of polarization switching of the fundamental longitudinal and transverse spatial modes in VCSEL's that we explore in this paper.

It is generally argued that the orientations of linearly polarized emissions are determined by the crystal axes which lead to birefringence and differences in surface reflectivities [8], [9], though stress-induced birefringence [10], [11] (from growth processes, electrical contacts, or deliberate damage) has also been noted. The birefringence gives different optical frequencies to the emissions with different linear polarizations. In some cases, the two frequencies are unresolved within experimental accuracy (<2–3 GHz) [3], [4], [12]. In other cases, the reported splittings are about 10–12 GHz [2], [5], [9] while a wide range (3–22 GHz) has also been reported [8].

Choquette *et al.* [10] have recently completed a careful study of the operation of VCSEL's as the mean of the frequencies of the two polarization modes is shifted from one side of the gain curve to the other and as the strain-induced anisotropies are varied, changing both the frequency splitting and the gain differences for the modes. These experimental results indicate that when the gain differential is large there is single-mode operation without switching, while when the gain differential is small there are two peaks in the emission spectrum near threshold, and polarization switching of the dominant emission state can be observed. Since the gain is a function of wavelength (VCSEL gain profiles are reportedly about 50 nm in width [13] and there is typically not more than 1-nm difference between the frequencies for the peak gains of the orthogonally polarized modes [14]), the birefringence-induced splitting of the mode frequencies leads to different gains for the two modes. Selection of a particular linearly polarized mode is then explained by the argument that the mode favored by the higher gain suppresses the mode with weaker gain. Switching of the polarization as the current is increased is explained by the shift in the gain profiles as functions of wavelength because of changes in the carrier

density and heating of the material. In addition, the resonant frequencies of the longitudinal modes shift with changes in the injection current because heating changes the cavity length and changes the index of refraction through changes in the carrier number. If the shifting gain profiles and cavity resonance frequencies lead to an exchange of the relative gain of the two modes, then a switching is expected [5], [10].

However, since the reported splittings of the frequencies of the linearly polarized modes involved in polarization switchings are in many cases less than 0.5% of the gain bandwidth, the gain differentials are often small. We investigate in this paper the effects of saturable dispersion and birefringence on mode stability and polarization switching when the modes have either the same, or only slightly different, gains. We find conditions under which a laser may select and maintain emission on the state of linear polarization which has the lesser gain. (A preliminary report of several of these results was presented in [15], [16].) Saturable dispersion which can cause this counterintuitive result is a natural part of semiconductor laser physics, and it is represented by the α factor in semiconductor rate equations [17]–[19] which indicates the dependence of the index of refraction on the carrier number.

The importance of saturable dispersion to polarization-state selection should be no surprise, since it was clearly established as a key factor in the polarization-state selection and polarization switchings of single-mode gas lasers. While a gain differential for linearly polarized emissions clearly plays a large role in polarization state selection, studies of third-order Lamb theories with equal gains for the two linear polarizations found that birefringence together with saturable dispersion is sufficient to explain many of the experimentally observed phenomena [20]–[23].

The outline of the paper is as follows. We first review in Section II a model for polarization dynamics in VCSEL's based on the angular momentum dependence of the conduction and valence bands of the semiconductor. The model incorporates birefringence and amplitude anisotropies for two linearly polarized modes. Section III describes the polarization states predicted by the model and their stability when the gain is the same for both modes. Polarization switching phenomena is anticipated by representing domains of stability of the linearly polarized modes in the parameter space of injection current and birefringence in Section IV. Switchings found by numerical integration of the model equations as the injection current is increased are discussed for particular parameter values. The polarization switching changes when there are small anisotropies in the gain or loss, and these are considered in Section V. Section VI presents results for the effects of the transverse spatial variation of the fundamental mode neglected in the previous sections, showing that there are no qualitative differences in the polarization-state selection and switching. Finally, Section VII presents results from our model for polarization switching or dynamical hysteresis induced by an injected optical signal.

II. A MODEL FOR POLARIZATION DYNAMICS IN VCSEL'S

The polarization state of light emitted by a laser depends on two main ingredients. The first is the angular momentum of the quantum states involved in the material transitions for emission or absorption. Emission of a quantum of light with right (left) circular polarization corresponds to a transition in which the projection of the total material angular momentum on the direction of propagation changes by $+1$ (-1) in units of $\hbar$. This first ingredient of polarization selection reflects the material dynamics of the different lasing transitions. The second ingredient is associated with the laser cavity. The anisotropies, geometry, and waveguiding effects of the cavity lead to a preference for a particular polarization state of the laser light. These two ingredients can compete or be complementary, their relative importance depending on the type of laser. Different atomic gas lasers emit linearly, circularly, or elliptically polarized light, and such polarization states have been identified with different atomic or molecular optical transitions [22]–[31]. The effect of cavity anisotropies has also been characterized for gas lasers [20].

Conventional edge emitting semiconductor lasers usually emit TE linearly polarized light due to the geometrical design of the laser cavity. Special engineering of the geometries, reflectivities, or the crystal stresses can favor TM linearly polarized light. The situation for surface-emitting lasers is more subtle, since they are found to emit linearly polarized light in a direction either randomly oriented in the plane of the active region (perpendicular to the direction of laser emission) or with preference for one or the other of two orthogonal directions in that plane. For these lasers, both of the ingredients discussed above should be important. The engineering for polarization control presently focuses on the modification of the cavity properties to stabilize a given polarization direction, but a better understanding of the intrinsic mechanisms of polarization selection may be useful for achieving improved or alternative methods of polarization control.

In view of these considerations, we discuss here a model [32] for the polarization dynamics of surface-emitting lasers which incorporates the cavity and material properties and which takes fully into account the phase dynamics of the electric field. In order to describe the angular momentum dependence of the electron-hole recombination process in a semiconductor, we recall [33] that near the band gap, the electron states of the conduction band have a total angular momentum quantum number $J = 1/2$. The upper valence bands are commonly known as heavy hole and light hole. For bulk material, the heavy hole and light hole bands are degenerate at the center of the band gap with a total angular momentum quantum number $J = 3/2$. For quantum wells, the quantum confinement removes this degeneracy. In the case of unstrained quantum wells, the heavy hole band, which is associated with $J_z = \pm 3/2$, has a higher energy. We consider a surface emitting quantum-well laser and we neglect transitions from the conduction to the light hole band. In this situation, the quantum allowed transitions are those in which $\Delta J_z = \pm 1$. We are then left with two allowed transitions between the conduction band and the heavy hole band: the transition from $J_z = -1/2$ to $J_z = -3/2$ is associated with right circularly polarized light and the transition from $J_z = 1/2$ to $J_z = 3/2$ is associated with left circularly polarized light. In a first approximation to semiconductor
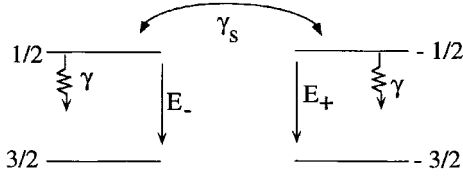
Fig. 1. Four-level model for polarization dynamics in quantu-well VCSEL's.

polarization dynamics, we can describe these transitions by the four-level model depicted in Fig. 1. For this model, the natural variables for the vector electric field amplitude are the slowly varying amplitudes $E_{\pm}$ of the left($-$) and right($+$) circularly polarized basis states which multiply carrier waves taken to be of the form $e^{-i(kz-\omega t)}$. Maxwell–Bloch equations for coupling these field variables to the material transitions have been developed [32]. A reduction of those equations leads to the following model, which can also be written down directly from Fig. 1 by general rate equation arguments supplemented with the introduction of phase dynamics:

$$\frac{dE_{\pm}}{dt} = -\kappa E_{\pm} - i\omega_0 E_{\pm} + \kappa(1+i\alpha)(N \pm n)E_{\pm} \tag{1}$$

$$\frac{dN}{dt} = -\gamma(N-\mu) - \gamma(N+n)|E_+|^2 - \gamma(N-n)|E_-|^2 \tag{2}$$

$$\frac{dn}{dt} = -\gamma_s n - \gamma(N+n)|E_+|^2 + \gamma(N-n)|E_-|^2. \tag{3}$$

In the four-level Maxwell–Bloch language, the laser light field is coupled to two population inversion variables: N is a normalized value of the sum of the upper state populations minus the sum of the lower state populations and n is a normalized value of the difference between the population inversions (upper and lower state population differences) on the two distinct channels with positive or negative values of J_z. In semiconductor language, the variable N represents the total carrier number in excess of its value at transparency, normalized to the value of that excess at the lasing threshold. The variable n represents the difference in the carrier numbers of the two magnetic sublevels normalized in the same way as N. While not immediately evident, there is an important subtle effect of n on the cross-saturation coupling of the right and left circularly polarized field amplitudes which might seem to interact independently with the two lasing transitions.

Physical parameters of these equations are the following: α is the linewidth enhancement factor, $\omega_0 = \kappa\alpha$ is a chosen shift in the optical carrier frequency that leads to zero frequency for the complex field amplitude at the lasing threshold, and μ is the normalized injection current which takes the value 1 at the lasing threshold. The model includes several decay rates: κ is the decay rate of the electric field in the cavity ($1/2\kappa$ is sometimes called the photon lifetime in the cavity), and γ is the decay rate of the total carrier number. The excess in the decay rate γ_s over γ accounts for the mixing of the carriers with opposite value of J_z.

For our purposes, the parameter γ_s can be understood as a phenomenological modeling of a variety of complicated microscopic processes, which are loosely termed spin-flip relaxation processes (actually population equilibration of the magnetic sublevels). Several spin relaxation processes for electrons and holes have been identified in semiconductors [34]–[38], e.g., scattering by defects [39], [40], exchange interactions between electrons and holes [41], and exciton-exciton exchange interactions [42]. From experimental measurements [36]–[38] of spin relaxation times in quantum wells, it is known that γ_s^{-1} is of the order of tens of picoseconds. Since typically $\gamma^{-1} \approx 1$ ns, and $\kappa^{-1} \approx 1$ ps [43], [44], the spin mixing described by γ_s occurs on an intermediate time scale between that of the field decay and that of the total carrier population difference decay. Hence, the dynamics of n cannot be adiabatically eliminated for the time scales of interest here.

In the mathematical limit of very large γ_s, n quickly relaxes to zero and one then obtains equations in which the two modal amplitudes $E_{\pm}$ are coupled to a single carrier population N, a model that is sometimes assumed phenomenologically for dual-polarization semiconductor lasers. This limit corresponds to a very fast mixing of populations with different spins in which the spin dynamics can be adiabatically eliminated. On the other hand, when γ_s takes on its minimum value given by the radiative lifetime of the carriers (i.e., when $\gamma_s = \gamma$), the right and left circularly polarized transitions are decoupled and two sets of independent equations for $(E_+, N_+ = N+n)$ and $(E_-, N_- = N-n)$ emerge.

We next turn to the consideration of the effects of cavity anisotropies which can be modeled in the two equations for the time evolution of the field amplitudes by replacing the linear loss rate κ by a matrix whose hermitian part is associated with amplitude losses and whose antihermitian part gives linear and circular phase anisotropies (also known as birefringence and circular dichroism, respectively). For VCSEL's, it is known that there are often two preferred modes of linear polarization that coincide with the crystal axes. These two modes have a frequency splitting associated with the birefringence of the medium. This can be modeled by a linear phase anisotropy, given by parameter γ_p, which represents the effect of a different indexes of refraction for the orthogonal linearly polarized modes. In addition, the two modes may have a slightly different gain-to-loss ratio that can be related to the anisotropic gain properties of the crystal [6], [45], the slightly different position of the frequencies of the modes with respect to the gain versus frequency curve [10], [46], and/or different cavity geometries for the differently polarized modes [2], [47]. These effects can be modeled by an amplitude anisotropy with parameter γ_a. We assume here for simplicity that the directions of linear phase and amplitude anisotropy coincide, so that both are diagonalized by the same basis states.

Incorporating the linear phase anisotropy and the linear amplitude anisotropy in (1) leads to

$$\frac{dE_{\pm}}{dt} = \kappa(1+i\alpha)(N \pm n - 1)E_{\pm} - i\gamma_p E_{\mp} - \gamma_a E_{\mp} \tag{4}$$

while the equations for N and n remain unchanged.

The meaning and effect of the parameters γ_p and γ_a are most clearly displayed when these equations are rewritten in terms of the orthogonal linear components of the electric field:

$$E_x = \frac{E_+ + E_-}{\sqrt{2}}, \quad E_y = -i\frac{E_+ - E_-}{\sqrt{2}}. \tag{5}$$

For the $\hat{x}$- and $\hat{y}$-polarized components the complete model becomes

$$\frac{dE_x}{dt} = -(\kappa + \gamma_a)E_x - i(\kappa\alpha + \gamma_p)E_x$$
$$+ \kappa(1 + i\alpha)(NE_x + inE_y), \qquad (6)$$

$$\frac{dE_y}{dt} = -(\kappa - \gamma_a)E_y - i(\kappa\alpha - \gamma_p)E_y$$
$$+ \kappa(1 + i\alpha)(NE_y - inE_x), \qquad (7)$$

$$\frac{dN}{dt} = -\gamma[N(1 + |E_x|^2 + |E_y|^2) - \mu$$
$$+ in(E_yE_x^* - E_xE_y^*)], \qquad (8)$$

$$\frac{dn}{dt} = -\gamma_s n - \gamma[n(|E_x|^2 + |E_y|^2)$$
$$+ iN(E_yE_x^* - E_xE_y^*)]. \qquad (9)$$

It is clear here that γ_p leads to a frequency difference of $2\gamma_p$ between the $\hat{x}$- and $\hat{y}$-polarized solutions (with the $\hat{x}$-polarized solution having the lower frequency when γ_p is positive) and that γ_a leads to different thresholds for these linearly polarized solutions with the $\hat{y}$-polarized solution having the lower threshold when γ_a is positive.

The values of these parameters depend critically on VCSEL designs, which range from etched posts to buried structures. Both index-guiding and gain-guiding structures have been fabricated. We use a generic model and reasonable parameter values.

The eigenstates of the system are linearly polarized (rather than circularly or elliptically polarized) because of the cross-saturation preference exerted through the nontrivial value of γ_s. However, the orientation of the linear polarization is not fixed by the nonlinear field-matter interaction in this model. Any amount of linear birefringence or linear gain anisotropy resulting from material or cavity anisotropies (and represented by nonzero values of γ_p and γ_a, respectively), restricts the linearly polarized solutions to one of two specific states polarized in the $\hat{x}$ and $\hat{y}$ directions.

In the absence of saturable dispersion ($\alpha = 0$) or birefringence ($\gamma_p = 0$), the anisotropic gain fully controls the stability of these two modes: the mode with the higher gain-to-loss ratio (which thereby has the lower threshold current) is always stable above its lasing threshold and the orthogonally polarized mode is always unstable when the solution exists (above a higher threshold value of the current). Without external injection of optical signals to excite and enforce operation of the unstable mode and without strong noise perturbations to induce temporary switchings to the unstable mode, simple variations of the injection current will not lead to polarization-state switching unless the gain anisotropy changes sign as the injection current is varied. Polarization switching will occur, without hysteresis, as the current crosses the value at which the gain anisotropy changes sign.

Semiconductor physics makes the saturable dispersion of the α factor unavoidable. Since birefringence also seems to be a common feature of VCSEL's, it is important that these properties be studied in conjunction with the gain anisotropy for their combined effect on polarization-state selection and polarization switchings. In addition, the dynamics of the magnetic sublevel populations provides a natural mechanism for enforcing the observed preference of these lasers for linearly polarized emission. In the remainder of this paper, we investigate the effects of these physical phenomena and show that many of the interesting polarization switchings (elsewhere attributed to gain anisotropies) can be explained as a consequence of birefringence and saturable dispersion.

III. POLARIZATION STATES AND THEIR STABILITY FOR ISOTROPIC GAIN

The model presented in Section II contains a variety of solutions with constant population variables, constant intensity, and a single optical frequency in their field spectra. We will call these stationary solutions because of their trivial time dependence that corresponds to an optical frequency shift. In order to obtain the analytical expressions for these solutions, we write an arbitrary steady state solution as

$$E_\pm = Q_\pm e^{i(\omega_\pm t \pm \psi) + i\theta}, \quad N = N_0, \quad n = n_0 \qquad (10)$$

where θ is an arbitrary phase that can be ignored, or set to zero, without loss of generality, and ψ is a relative phase.

In absence of anisotropies ($\gamma_a = \gamma_p = 0$) there are linearly polarized solutions [32] in which the amplitudes of the two circularly polarized components are equal and the frequencies are equal:

$$Q_\pm = \sqrt{\frac{\mu - 1}{2}}, \quad \omega_\pm = 0. \qquad (11)$$

The relative phase ψ is arbitrary and determines the orientation of the linear polarization. The projection of the linearly polarized field on the $x - y$ basis is given by

$$E_x = \sqrt{\mu - 1}\cos\psi, \quad E_y = \sqrt{\mu - 1}\sin\psi. \qquad (12)$$

While this solution is susceptible to orientational diffusion due to perturbations of the phase ψ, with respect to amplitude perturbations this state is linearly stable for any finite value of the parameters, but as $\gamma_s \to \infty$, it becomes marginally stable with respect to amplitude fluctuations [32]. This means that the finite value of γ_s for the isotropic case stabilizes the linearly polarized emission and destabilizes circularly polarized or elliptically polarized emission.

When $\gamma_p \neq 0$, and when there are no amplitude (gain or loss) anisotropies ($\gamma_a = 0$), we obtain four types of steady-state solutions (see Fig. 2). For each of these solutions, the phase anisotropy breaks the rotational invariance of the orientation of the field (polarization) vector, that is, the relative phase ψ is no longer arbitrary. Two of these types of solutions have orthogonal linear polarization. We will call these states the $\hat{x}$- and $\hat{y}$-polarized solutions (modes). For each of these modes, the circularly polarized components have equal amplitudes. The other two types of solutions are elliptically polarized for which the circularly polarized components have unequal amplitudes.

The $\hat{x}$ linearly polarized solution [shown in Fig. 2(a)] given by

$$Q_\pm = \sqrt{\frac{\mu - 1}{2}}, \quad \omega_\pm = -\gamma_p, \quad \psi = 0 \qquad (13)$$
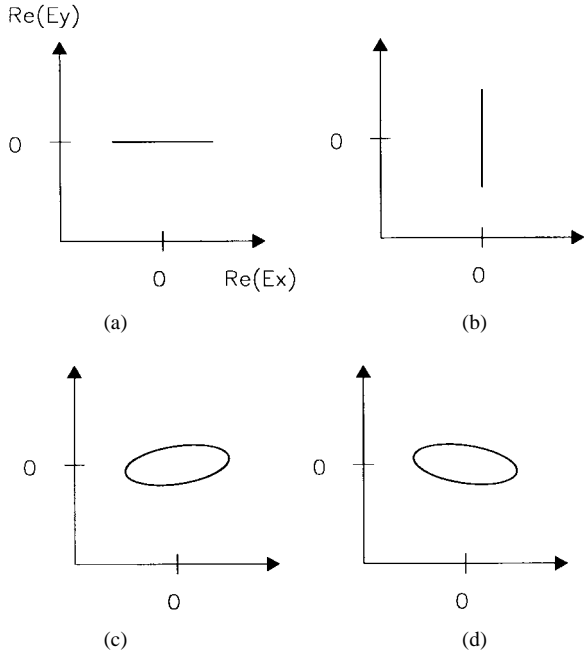
Fig. 2. Steady-state solutions of (6)–(9): (a) $\hat{x}$ polarized, (b) $\hat{y}$ polarized, and (c)–(d) elliptically polarized.

corresponds to

$$E_x = \sqrt{\mu - 1}e^{-i\gamma_p t}, \quad E_y = 0. \tag{14}$$

The $\hat{y}$-linearly polarized solution [shown in Fig. 2(b)] with

$$Q_\pm = \sqrt{\frac{\mu - 1}{2}}, \quad \omega_\pm = \gamma_p, \quad \psi = \frac{\pi}{2} \tag{15}$$

corresponds to

$$E_x = 0, \quad E_y = \sqrt{\mu - 1}e^{i\gamma_p t}. \tag{16}$$

The steady-state values of the total carrier population and the population difference between the sublevels with opposite value of the spin for both linearly polarized solutions are

$$N_0 = 1, \quad n_0 = 0. \tag{17}$$

The two elliptically polarized solutions are given by

$$Q_\pm^2 = \frac{1}{2}(\mu - N_0)\left(1 \mp \frac{N_0 - 1}{n_0}\right) \tag{18}$$

$$\omega_\pm = \kappa\alpha\frac{(N_0 - 1)^2 - n_0^2}{N_0 - 1} \tag{19}$$

$$\tan(2\psi) = \frac{1}{\alpha}\frac{N_0 - 1}{n_0}. \tag{20}$$

The two solutions are distinguished by the two values for the population difference n_0 which are given by

$$n_0^2 = \frac{(\mu - N_0)(N_0 - 1)N_0}{\gamma_s/\gamma + \mu - N_0}. \tag{21}$$

The value for N_0 is obtained by

$$\gamma_p^2\left(\frac{\gamma_s}{\gamma} + \mu - N_0\right)^2$$
$$= \kappa^2\left[\left(\left(\frac{\gamma_s}{\gamma} + \mu - N_0\right) - \frac{\gamma_s}{\gamma}N_0\right]\right.$$
$$\left. \cdot \left[\left(\frac{\gamma_s}{\gamma} + \mu - N_0\right)(N_0 - 1) + \alpha^2(\mu - N_0)N_0\right] \tag{22}$$

but (21) restricts the possible values to those for which N_0 is greater than 1. From (22), $N_0 > 1$ requires

$$\mu > 1 + \frac{\gamma_s\gamma_p}{\gamma(\kappa\alpha - \gamma_p)}. \tag{23}$$

An interesting result is obtained when $\gamma_p = 0$, for which each elliptically polarized solution becomes circularly polarized light. In this case, we have

$$N_0 = \frac{\mu + \frac{\gamma_s}{\gamma}}{1 + \frac{\gamma_s}{\gamma}}, \quad n_0 = \pm(N_0 - 1) \tag{24}$$

where the positive sign yields left circularly polarized light and the negative sign yields right circularly polarized light. However, these circularly polarized solutions are unstable for $\gamma_p = 0$ [32]. In general, for $\gamma_p \neq 0$, the relation $|n| \geq N - 1$ is always satisfied if (23) is verified. The two different elliptically polarized solutions have the same optical frequency but different orientations of their polarization ellipses and different senses of rotation [see Fig. 2(c)]. Elliptically polarized states have been experimentally found in VCSEL's with applied longitudinal magnetic fields. The remnant ellipticity for zero magnetic field is extremely small [48], [49].

In order to study the linear stability of these solutions, we have used a standard procedure. The stability of a particular solution is studied by writing this solution as

$$E_\pm = (Q_\pm + a_\pm)e^{i(\omega_\pm t \pm \psi)}$$
$$N = N_0 + \Delta$$
$$n = n_0 + \delta \tag{25}$$

where $a_\pm$ is a complex perturbation of the field amplitude, and Δ and δ are real perturbations related to the carrier variables.

After substituting the perturbed solution given by (25) in the equations of the model and linearizing to first order in the perturbation, one obtains the following set of linear coupled differential equations for $a_\pm, \Delta$, and δ:

$$\dot{a}_\pm = \kappa(1 + i\alpha)(N_0 \pm n_0 - 1)a_\pm - i\alpha\kappa a_\pm + \kappa(1 + i\alpha)$$
$$\cdot (\Delta \pm \delta)Q_\pm - i\gamma_p a_\pm e^{\mp i2\psi}$$
$$\dot{\Delta} = -\gamma(N_0 + n_0)Q_+(a_+ + a_+^*) - \gamma(N_0 - n_0)$$
$$\cdot Q_-(a_- + a_-^*) - \gamma(1 + Q_+^2 + Q_-^2)\Delta$$
$$- \gamma(Q_+^2 - Q_-^2)\delta$$
$$\dot{\delta} = -\gamma(N_0 + n_0)Q_+(a_+ + a_+^*) + \gamma(N_0 - n_0)$$
$$\cdot Q_-(a_- + a_-^*) - \gamma(Q_+^2 - Q_-^2)\Delta$$
$$- [\gamma_s + \gamma(Q_+^2 + Q_-^2)]\delta. \tag{26}$$

In order to simplify the notation, (26) is written in vectorial form as

$$\partial_t \vec{A} = \boldsymbol{M} \vec{A} \tag{27}$$

where $\vec{A} = (a_+, a_+^*, a_-, a_-^*, \Delta, \delta)$, and $\boldsymbol{M}$ is a 6×6 matrix whose coefficients can be easily derived from (26). The eigenvalues of $\boldsymbol{M}$ are determined by a sixth-order polynomial that has to be solved. The linear stability of a steady state solution is given by the real parts of the eigenvalues which indicate if the solution is stable (when $\mathrm{Re}(\lambda) < 0$ for all λ) or unstable (when $\mathrm{Re}(\lambda) > 0$ for at least one λ), while the imaginary part of λ, when it exists, gives a frequency characteristic of the evolution of the perturbation.

We first consider the stability of the linearly polarized solutions by substituting in (27) the steady-state solution for the linearly $\hat{x}$- and $\hat{y}$-polarized states given by (13) and (17) or (15) and (17), respectively. The set of equations given by (27) can be decoupled into two independent subsets if the equations are rewritten for the variables $S = a_+ + a_-$ and $R = a_+ - a_-$ as was done in [32]. The first subset is

$$\dot{S} = 2\kappa(1 + i\alpha)Q\Delta$$
$$\dot{S}^* = 2\kappa(1 - i\alpha)Q\Delta$$
$$\dot{\Delta} = -\gamma QS - \gamma QS^* - \gamma(1 + 2Q^2)\Delta \tag{28}$$

which determines the stability of a polarized solution with respect to perturbations with the same polarization. This subset of equations is independent of γ_p and γ_s. The general solution

$$\begin{pmatrix} S \\ S^* \\ \Delta \end{pmatrix} = \begin{pmatrix} S_0 \\ S_0^* \\ \Delta_0 \end{pmatrix} e^{\lambda \gamma t} \tag{29}$$

leads always to a zero eigenvalue, associated with the arbitrary global phase θ, and two complex conjugate eigenvalues with negative real parts. These complex eigenvalues are associated with ordinary relaxation oscillations characteristic of many lasers, including semiconductor lasers. This means that each linearly polarized steady-state solution is always stable with respect to amplitude perturbations with the same polarization.

The second subset of equations is

$$\dot{R} = 2\kappa(1 + i\alpha)Q\delta \pm i2\gamma_p R$$
$$\dot{R}^* = 2\kappa(1 - i\alpha)Q\delta \mp i2\gamma_p R^*$$
$$\dot{\delta} = -\gamma QR - \gamma QR^* - (\gamma_s + 2\gamma Q^2)\delta \tag{30}$$

where the lower sign is for the stability of the linearly $\hat{x}$-polarized steady-state solution and the upper sign is for the stability of the linearly $\hat{y}$-polarized one. This subset determines the stability of a polarized solution with respect to perturbations of the orthogonal polarization. For $\gamma_p = 0$, there is a zero eigenvalue associated with the arbitrariness of the polarization direction, and there are two more eigenvalues that always have negative real parts [32]. These two eigenvalues are complex for small γ_s, describing polarization relaxation oscillations. These eigenvalues become real for large γ_s and one of them approaches zero as $\gamma_s \to \infty$ [32], corresponding to the existence of (and diffusion among) a family of elliptically

polarized states with arbitrary ellipticity. When $\gamma_p \neq 0$, the zero eigenvalue becomes nonzero, thus stabilizing or destabilizing a given steady state. To determine the eigenvalues of (30), we set

$$\begin{pmatrix} R \\ R^* \\ \delta \end{pmatrix} = \begin{pmatrix} R_0 \\ R_0^* \\ \delta_0 \end{pmatrix} e^{\lambda \gamma t}. \tag{31}$$

The resulting third-order polynomial for λ is

$$\begin{aligned} P(\lambda) = \lambda^3 &+ \left(\frac{\gamma_s}{\gamma} + \mu - 1 \right) \lambda^2 \\ &+ \left[2\frac{\kappa}{\gamma}(\mu - 1) + 4\left(\frac{\gamma_p}{\gamma}\right)^2 \right] \lambda \\ &+ 4\left(\frac{\gamma_p}{\gamma}\right)^2 \left(\frac{\gamma_s}{\gamma} + \mu - 1 \right) \mp 4\frac{\kappa \gamma_p}{\gamma^2}\alpha(\mu - 1) \end{aligned} \tag{32}$$

where the upper sign holds for the stability of the linearly $\hat{x}$-polarized solution, while the lower sign holds for the stability of the linearly $\hat{y}$-polarized one. The stability of the linearly polarized solutions, is then, strongly determined by the zeroth-order term of (32). The amplitudes, frequencies, and stabilities of the $\hat{x}$- and $\hat{y}$-polarized solutions can be interchanged by changing the sign of γ_p.

It is interesting to consider first the ideal situation in which there is no saturable dispersion in the field-matter interaction. In semiconductor physics language, this would be a case of no amplitude-phase modulation (no coupling between amplitude fluctuations and frequency fluctuations) in which $\alpha = 0$. In this case, both linearly polarized solutions are always stable (the coefficients of the polynomial are all positive), so that there exists a regime of bistability for any value of μ or γ_p. Therefore, for $\alpha = 0$, no polarization switching occurs as the injection current is changed. However we show below that the nonvanishing value of α, together with the phase anisotropy, causes polarization switching. This is the same type of behavior known for gas lasers, where for zero detuning, both linearly polarized modes are stable for any value of the birefringence parameter, but polarization switching occurs for nonzero detuning.

We determine the stability of a particular solution for a general value of α in terms of two control parameters, the injection current μ and the birefringence parameter γ_p/γ, which are commonly measured in polarization switching experiments. The lines separating stability regions in this parameter space are those for which $\lambda = 0 + i\nu$. For the $\hat{x}$-polarized solution, the critical value of μ at which the stability of this solution changes is given by

$$\mu_x = 1 + \frac{\gamma_s \gamma_p}{\gamma(\kappa \alpha - \gamma_p)} \tag{33}$$

with $\nu = 0$ so that the eigenvalue which vanishes at this line is real, indicating that any $\hat{y}$-polarized perturbation presents pure exponential growth or decay in the neighborhood of μ_x. This eigenvalue, which becomes zero at $\mu = \mu_x$ for $\gamma_p > 0$, is the eigenvalue which is identically zero for $\gamma_p = 0$. The other two eigenvalues with negative real parts for $\gamma_p = 0$ have negative
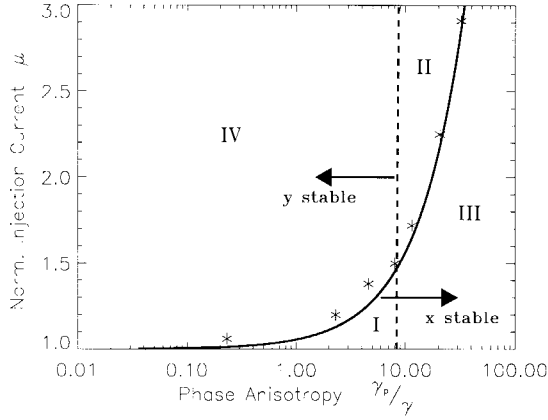
Fig. 3. Stability diagram for the steady-state solutions. The $\hat{x}$-polarized state is stable below the continuous line, while the $\hat{y}$-polarized state is stable to the left of the dashed line. This divides this parameter space into four zones with different stability for the two linearly polarized solutions: in I, both solutions are stable; in II, neither solution is stable; in III, only the $\hat{x}$-polarized solution is stable; and in IV, only the $\hat{y}$-polarized solution is stable. Elliptically polarized solutions are stable within the narrow region between the solid line and the stars. The following parameters have been used: $\kappa = 300$ ns^{-1}, $\gamma = 1$ ns^{-1}, $\gamma_s = 50$ ns^{-1}, and $\alpha = 3$.

real parts for any value of μ and $\gamma_p > 0$. In summary, the $\hat{x}$-polarized solution is always stable for any $\mu < \mu_x$, which occurs below the solid line plotted in Fig. 3.

In the same way, for the $\hat{y}$-polarized solution, one obtains the instability curve

$$\mu_y = 1 - \frac{\gamma_s}{\gamma} + 2\alpha\frac{\gamma_p}{\gamma}. \tag{34}$$

The $\hat{y}$-polarized solution is stable when $\mu > \mu_y$, which occurs to the left of the dashed line in Fig. 3. In this case, the eigenvalue which becomes unstable is complex and $\hat{x}$-polarized perturbations present exponential growth or decay with oscillations at a frequency given by

$$\nu = [4\gamma_p^2 + 2\kappa(2\alpha\gamma_p - \gamma_s)]^{1/2} \tag{35}$$

when $\mu = \mu_y$. The instability governed by this complex eigenvalue can have two different regimes as γ_p increases, from $\gamma_p = 0$. For small γ_s, the complex eigenvalue has a positive real part while the identically zero eigenvalue at $\gamma_p = 0$ becomes a real and negative number. On the other hand, for large γ_s, the origin of the instability is that, starting from $\gamma_p = 0$, as γ_p increases the zero eigenvalue and a real eigenvalue collide, creating a pair of complex conjugate eigenvalues with a real part which becomes positive as γ_p increases.

The parameter space is divided by (33) and (34) into four different regions with different stability for the linearly polarized solutions. This is shown in the stability diagram of Fig. 3: region I, where both linearly polarized states are stable, region II, where both are unstable, and regions III and IV, where only $\hat{x}$- or $\hat{y}$-polarized solutions are stable, respectively. For realistic values of the parameters used in Fig. 3, the stability diagram is a consequence of the combined effect of saturable dispersion associated with the α-factor and spin dynamics associated with a finite value of γ_s. We note again

that the relative stability of the $\hat{x}$- or $\hat{y}$-polarized solutions can be interchanged by changing the sign of γ_p.

As we have already discussed, only region I survives when phase-amplitude modulation is neglected by setting $\alpha = 0$. Therefore, region IV appears as a consequence of saturable dispersion which favors the $\hat{y}$-polarized mode with a small positive frequency shift induced by birefringence. On the other hand, the existence of region II, where it might be possible for the two polarizations to coexist, is a consequence of spin dynamics. Indeed, in the mathematical limit of very large γ_s, in which the dynamics of n can be eliminated in the description because of very fast spin relaxation, the dashed line determined by (34) moves to higher values of the birefringence parameter, while keeping its slope $2\alpha/\gamma$, so that for finite pumping, it does not cross the line $\mu = \mu_x$. In the same limit, the solid line becomes very steep, but for any finite value of γ_s there is always a domain in which only the $\hat{y}$-polarized solution is stable for large enough pumping or small enough γ_p.

A better understanding of the role of spin-dynamics in the stability diagram of Fig. 3 is obtained considering (2)–(4) in the limit $n = 0$. In this limit of extremely fast mixing of carrier population with different J_z, there is an eigenvalue with a zero real part, indicating that R in (30) is marginally stable. This indicates that there is no preference for linear or circularly polarized light. From a formal point of view, this fact also becomes clear in a third-order Lamb theory obtained from (2) to (4) by adiabatic elimination of N and n in the limit $\gamma_s, \gamma \to \infty$ with $\rho = \gamma_s/\gamma$ finite. We find

$$\partial_t E_\pm = -(\gamma_a + i\gamma_p)E_\mp$$
$$\cdot \kappa(1+i\alpha)\left(\mu + \frac{\mu}{\rho}\right)\left[\frac{\mu-1}{\mu+\frac{\mu}{\rho}} - |E_\pm|^2 - \delta|E_\mp|^2\right]E_\pm \tag{36}$$

where the coupling parameter is $\delta = (\rho - 1/\rho + 1)$. For weak coupling ($\delta < 1$), there is a preference for linearly polarized emission, while for large coupling ($\delta > 1$), there is a preference for circular polarization. The limiting cases here are $\rho \to 1$, giving light strongly linearly polarized, and $\rho \to \infty$ (fast spin relaxation) in which there is marginal coupling ($\delta = 1$).

Finally, the linear stability of elliptically polarized solutions has also been examined. In this case, the values of $Q_\pm, \omega_\pm, \psi$, and n_0 are given by (18)–(21) after solving (22) for N_0. However, the particular values of the steady state do not allow decoupling (27) into the subsets for (S, S^*, Δ) and (R, R^*, δ), as was done for the linearly polarized solutions. This forces us to work directly with a sixth-order polynomial for the eigenvalues. To find the stability of a particular elliptically polarized solution, we numerically obtain the values of the coefficients of the polynomial and then we find their eigenvalues. The stability is determined by looking at the real part of the eigenvalue as previously described. The procedure has been applied to several values of the birefringence parameter for the range of injection current shown in the stability diagram of Fig. 3. We have indicated on the figure by stars, the values of μ and γ_p/γ that verify Re $(\lambda) = 0$. The elliptically polarized solution is stable in a narrow domain of parameters in which

μ is close to but larger than μ_x. Note that according to (23), this solution only exists for $\mu > \mu_x$.

IV. INJECTION CURRENT SCANS AND POLARIZATION SWITCHING FOR ISOTROPIC GAIN

In experiments on polarization switching in VCSEL's, it is common to measure the optical power of each of the linearly polarized modes as the injection current is increased. The frequency difference between the modes remains constant as the injection current is varied [8]. These experimental conditions and constraints can be reproduced in our model by varying the injection current while holding the birefringence parameter fixed, that is, by moving vertically in the parameter space of Fig. 3. To see the resulting dynamics and changes in the polarization state, we numerically integrated (1)–(3) in time with weak stochastic noise perturbations (of strength $\beta = 10^{-4} \, \text{s}^{-1}$) added to each of the variables as in [50]. The injection current was periodically increased in small abrupt steps (5% of the threshold value), beginning from a value of the injection current which started the laser below threshold. Each new value of the current was held constant for a time interval equivalent to about 40 ns, long enough in most cases to ensure that the transient evolution of the fields and carriers was almost completely finished. Fig. 4 shows an example of the temporally stepped injection current and the resulting evolution and changes in the intensities of each linearly polarized mode and in the carrier numbers. The final states in the time ranges #1 and #6 (indicated on the figure) correspond to linearly $\hat{x}$- and $\hat{y}$-polarized emission, respectively. In time ranges #2 and #3, the final state is elliptically polarized. Solutions with periodic modulation of the variables corresponding to states of mixed polarization were found in time ranges #4 and #5.

If we assume that the laser will most often settle on an available stable steady-state solution, Fig. 3 allows us to predict polarization switching when the injection current is varied, as these variations can move the laser from a zone where one linearly polarized mode is stable to a zone where the other linearly polarized mode is stable. From Fig. 3 alone, it is not clear how, or whether, the elliptically polarized steady states would be involved in these transitions.

We first consider a scan of the injection current in the domain where $\hat{y}$-polarized emission is always stable, that is, for small values of the birefringence parameter. "Small" in this case is determined by having frequency splittings between the linearly polarized modes that are less than the typical relaxation rate of the population differences in the magnetic sublevels (spin relaxation rate). In this case, just above threshold there is bistability of the two linearly polarized solutions. Spontaneous emission noise fluctuations as the laser is brought from below threshold to above threshold will set the initial conditions that select one of the two linearly polarized modes. Just above threshold there would be a slightly greater likelihood of finding the more stable ($\hat{y}$-polarized) mode because of noise-induced switching. The time evolution as the current is increased depends on which mode is initially selected: 1) if the system begins with a $\hat{y}$-polarized solution,
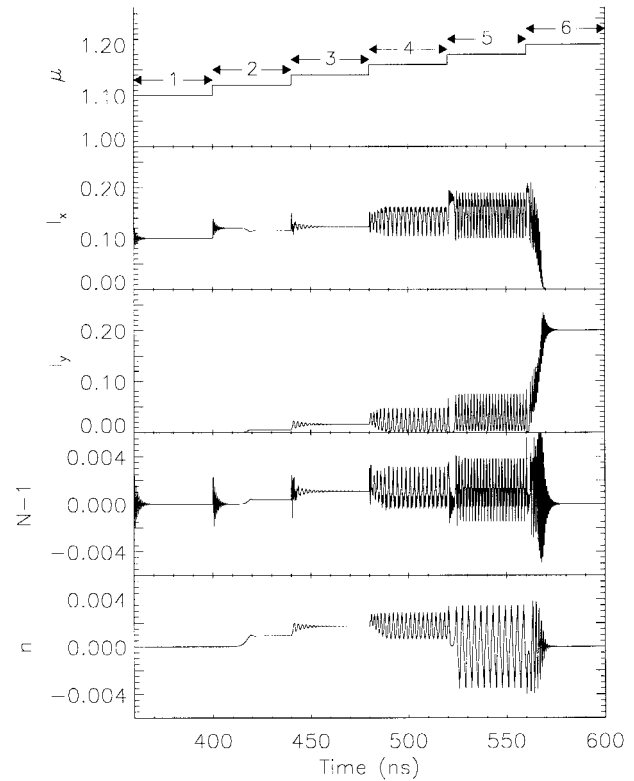

Fig. 4. Time-dependent evolution of the injection current (increased in steps), the intensities of each polarized mode ($I_x = |E_x|^2$, $I_y = |E_y|^2$), and the carrier variables N and n, when the injection current μ is increased. The parameters used are those of Fig. 3 and $\gamma_p = 2\gamma$.

this polarization mode is retained as μ is raised and lowered because it is stable for the whole range of injection currents or 2) if the system begins with $\hat{x}$-polarized emission, it will switch from $\hat{x}$-polarization at a value of the injection current given by $\mu = \mu_x(\gamma_p)$ and is likely to be found in the $\hat{y}$-polarized mode when μ is further increased enough that $\hat{y}$-polarized emission is the only stable steady state. Once the laser reaches $\hat{y}$-polarized emission, this new state will be retained stably if the injection current is raised further, or if it is lowered, even if it is lowered into the bistable region. This would provide an evident "one-time" hysteresis signature which would not be repeated as the injection current was raised and lowered unless the laser again, due to spontaneous emission noise or other fluctuations, switched stochastically to the $\hat{x}$-polarized mode in the bistable region or when the laser was operated below the lasing threshold.

Results for a scan of the injection current with a fixed value $\gamma_p = 2\gamma$, which is midway in the zone that is initially bistable, are shown in Fig. 5. In order to compare this result with the experimental results which are typically completed with a slow (quasi-adiabatic) scan of the injection current, the intensity was averaged during the last 20 ns (second half) of each time interval during which the injection current was held at a particular value. The averaged intensity for each linearly polarized mode is plotted versus the value of the injection current, giving a light–current characteristic for each polarized mode. (This procedure was followed rather than a quasi-adiabatic scan of the current which could be fashioned from a
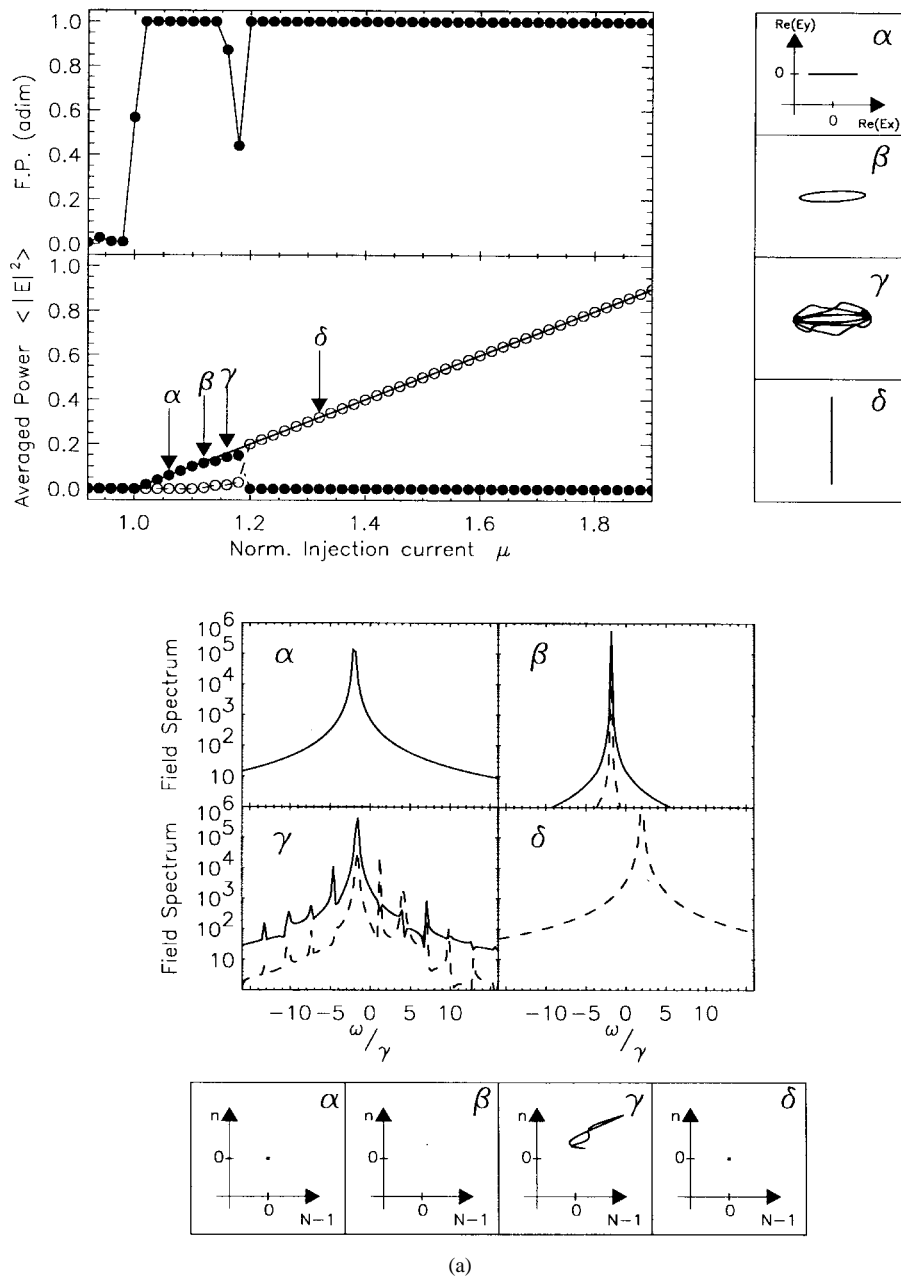
(a)

Fig. 5. (a) Light–current characteristic for the intensity of each linearly polarized mode (solid dots: $\hat{x}$-polarized; open circles: $\hat{y}$-polarized) and the associated fractional polarization (FP). $\mathrm{Re}\,(E_x)$ versus $\mathrm{Re}\,(E_y)$ plots, $N - 1$ versus n, and optical spectra of the field amplitudes E_x (solid line) and E_y (dashed line) for the solutions labeled on the light–current characteristic.

series of many smaller steps, in order to allow transients to die out and to avoid the phenomena which result from scanning a parameter through a bifurcation point with the consequent critical slowing [51]–[53]. Of course, in detailed comparisons with experiments with continuously scanned currents, such critical phenomena must be present and one would also have to include adequate noise strengths in all variables to make an accurate prediction.)

As expected, two different light–current characteristics were obtained, depending on which of the two stable steady states was selected as the laser was brought above threshold. When the initial selected state was $\hat{y}$-polarized, this state was retained for any value of the injection current. As this is a relatively trivial result for presentation, it is not represented in Fig. 5.

Instead, Fig. 5(a) shows the light–current characteristic for the other case, when the selected initial state is $\hat{x}$-polarized. The $\hat{x}$-polarized state is retained up to $\mu = 1.1$ where it loses its stability to elliptically polarized emission. After a further increase in the injection current, the output changes to the $\hat{y}$-polarized state at $\mu = 1.2$. The switching involves intermediate states of different polarization, such as an elliptically polarized state (an example is labeled by β) and some other complex time-dependent intensity solutions (an example is labeled by γ). Each emission state can be also characterized by the optical spectrum (spectrum of the electric field amplitude) which we compute for the last 20 ns of each transient for each of the linearly polarized states. For the linearly polarized state (α and δ) and the elliptically polarized state (β), the spectra
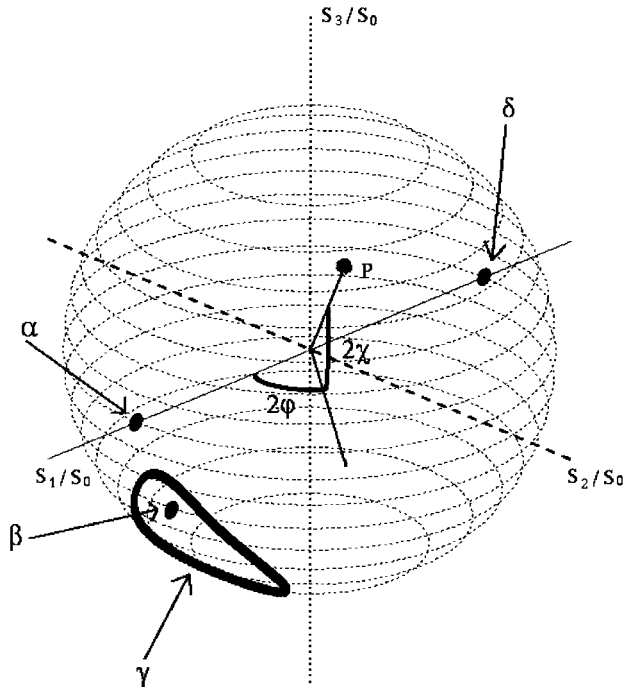
Fig. 5. *(Continued.)* (b) Time evolution of the labeled states on the normalized Poincare Sphere. The parameters are those of Fig. 3 and $\gamma_p = 2\gamma$.

have one well-defined peak. For the solution with time-varying intensities (γ), each of the spectra for the linearly polarized field amplitudes has a main peak (at the same frequency in the two cases) and many equally spaced sidebands, which is the signature of the periodic modulation of the intensity (and phase) for each component.

For a better description of these intermediate states, we use three alternative characterizations of the data from the last 20 ns of each current step: first a plot of $\text{Re}(E_x)$ versus the $\text{Re}(E_y)$ for a given time interval, secondly, the Poincaré sphere representation, and third, a measure of polarization given by the fractional polarization (FP). We have selected a particular example from each qualitatively different type of emission along the light–current characteristic curve in Fig. 5(a) (for example, α labels a condition of $\hat{x}$-polarized emission while δ labels a case with $\hat{y}$-polarized emission). The $\text{Re}(E_x)$ versus the $\text{Re}(E_y)$ plots are shown beside the light–current characteristics for the labeled states and clearly identify the different types of polarization; a curve or line is obtained because the solutions have a nonzero optical frequency relative to the rotating reference frame selected for the slowly varying amplitudes of the model. This kind of plot represents the projection of our six-dimensional space of dynamical variables onto a two-dimensional space, and some information is necessarily lost or obscured.

An alternative two-dimensional plot is that of one carrier variable (N) versus the other one (n). For the steady states (constant intensity solutions, both linearly and elliptically polarized), both carrier variables are time independent, resulting in a single point in the plot as given by (17) or (21) and (22), respectively. Finally, the time dependence of the carrier variables for the case labeled as γ reflects the lack of a well-

defined state of polarization. However, a closed trajectory is obtained which indicates a distinct relation between the two carrier magnitudes and an overall periodic evolution. For comparisons, the behavior labeled γ in Fig. 5(a) corresponds to the time range #4 in Fig. 4.

Another way to characterize the polarization of a state is the Poincaré sphere plot [22], as in Fig. 5(b), where for the given pair of field amplitudes $(E_+(t), E_-(t))$ we assign the radial value of a point on the trajectory $(\rho_0^2(t))$ to the total intensity of this state; the azimuth angle on the Poincaré sphere is given by $2\varphi(t)$, where φ is the angle of the instantaneous polarization in the x-y plane; and the polar angle, $2\chi(t)$, of the point on the Poincaré sphere is set by χ which is the instantaneous ellipticity of the emission. These quantities appear in the definition of the Stokes parameters:

$$
\begin{aligned}
s_0(t) &= |E_+(t)|^2 + |E_-(t)|^2 = \rho_0^2(t) \\
s_1(t) &= 2\,\text{Re}\,(E_+(t)E_-^*(t)) = \rho_0^2(t)\cos(2\chi(t))\cos(2\varphi(t)) \\
s_2(t) &= 2\,\text{Im}\,(E_+(t)E_-^*(t)) = \rho_0^2(t)\cos(2\chi(t))\sin(2\varphi(t)) \\
s_3(t) &= |E_+(t)|^2 - |E_-(t)|^2 = \rho_0^2(t)\sin(2\chi(t)).
\end{aligned}
\tag{37}
$$

The Stokes parameters obey at every time the identity

$$
s_0(t)^2 = s_1(t)^2 + s_2(t)^2 + s_3(t)^2.
\tag{38}
$$

By identifying $s_i/s_0, i = 1, 2, 3$, with the cartesian coordinates x, y, and z, (38) can be regarded as the equation of the unit sphere. Every polarization state of the laser beam is then represented by a point on the surface of the sphere. In case of polarized light, the Stokes parameters are constant in time, since intensity, polarization, and helicity are fixed.

For incompletely polarized light, the Stokes parameters vary in time because the amplitudes E_+ and E_- and the relative phases vary. In this case, what one can do is to measure the averages $\langle s_i \rangle$ over a suitable time interval. In general, (38) must be replaced by the inequality

$$
\langle s_0 \rangle^2 \geq \langle s_1 \rangle^2 + \langle s_2 \rangle^2 + \langle s_3 \rangle^2
\tag{39}
$$

where the equals sign holds only for a state of pure polarization. A measure of the degree of polarization of a vector optical field is given by the FP, defined as [54]

$$
\text{FP} = \frac{\langle s_1 \rangle^2 + \langle s_2 \rangle^2 + \langle s_3 \rangle^2}{\langle s_0 \rangle^2}.
\tag{40}
$$

The FP ranges from 0 (natural unpolarized light) to 1 (polarized light), taking intermediate values for incompletely polarized light.

This new physical quantity can supply some of the information missing in the $\text{Re}(E_x)$ versus $\text{Re}(E_y)$ plots when the solutions are time dependent ($0 < \text{FP} < 1$). The values of the FP averaged over the last 20 ns of each current step are plotted above the light–current characteristic in Fig. 5(a). The linearly polarized and the elliptically polarized states have FP $= 1$, while the time-dependent states (of mixed polarization) have FP < 1. The Poincaré sphere representation of each of the four identified states ($\alpha, \beta, \gamma,$ and δ) is shown in Fig. 5(b). When the state has FP $= 1$ (states $\alpha, \beta,$ and δ), it is represented by a time-independent point on the sphere. This point lies on
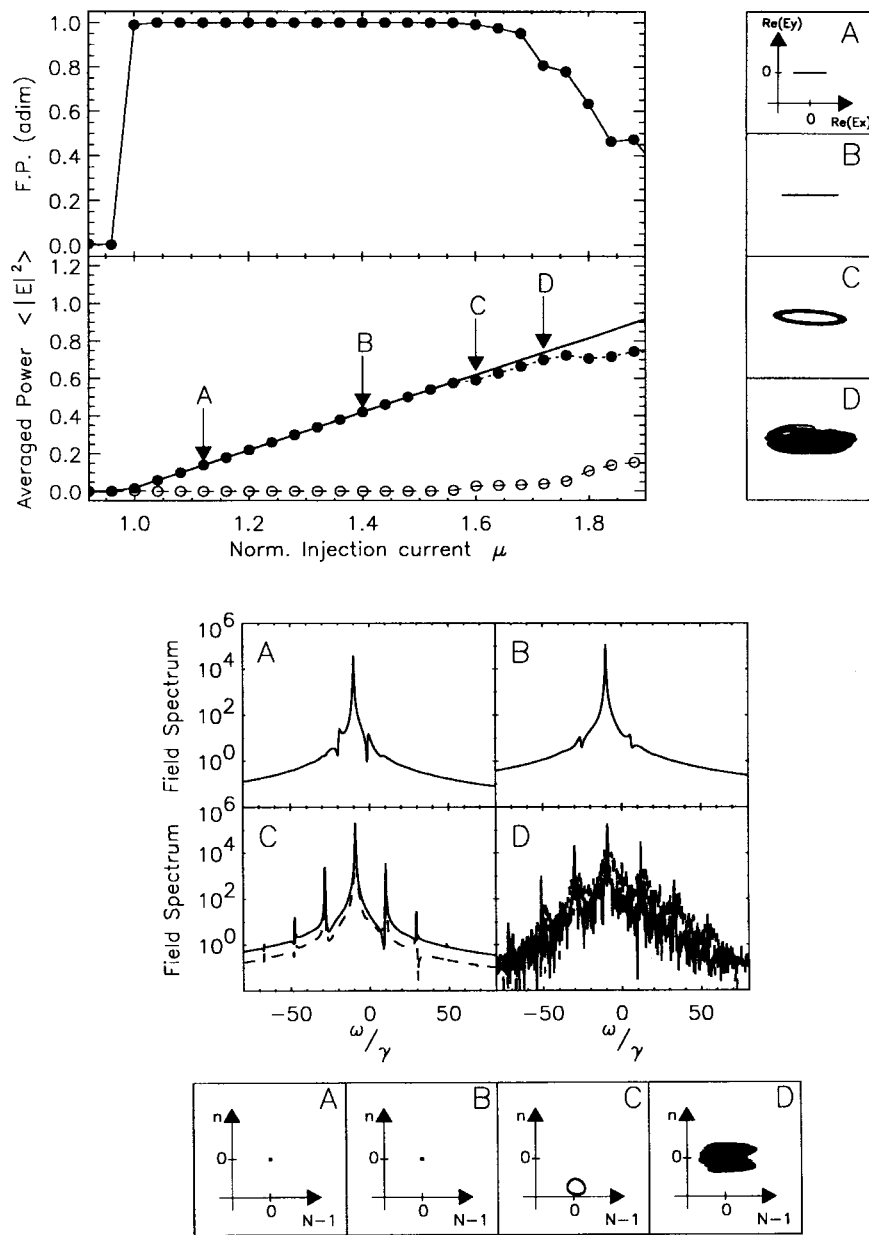
Fig. 6. Same as Fig. 5(a), but for $\gamma_p = 10\gamma$. The y scale of figure C in the $N - 1$ versus n plot has been expanded 20 times to increase the resolution.

the equator of the sphere if the state is linearly polarized. However, when the state has FP < 1, the representative point moves on the surface of the normalized sphere. When the intensities vary periodically the representative point moves on a closed trajectory (state γ). The state γ can be understood as an elliptically polarized state whose ellipticity and azimuth change in time in a periodic way. For states with a broad field spectrum (corresponding to quasi-periodic or chaotic variation of the intensities), the representative point would move in a complicated (not closed) trajectory on the surface of the sphere.

Elliptically polarized states are stable in a very narrow region. They can be understood as an intermediate stationary state reached in the destabilization by a steady bifurcation of a linearly polarized solution as the current is increased. At the critical value of the current at which the $\hat{x}$-polarized state

loses its stability, the elliptically polarized state appears as an infinitesimal distortion of the destabilized state. There are two frequency-degenerate elliptically polarized solutions with two possible signs for the azimuth [two orientations, see Fig. 2(c)]. The supercritical transition from one linearly polarized mode to the other can occur through either of these two states.

We next consider a scan of the injection current, at a fixed value of γ_p which is comparable to the relaxation rate of the magnetic sublevels, and, therefore, where sublevel population dynamics play a crucial role. For these values of γ_p, the $\hat{x}$-polarized state is the only stable steady state near the lasing threshold, but no linearly polarized state is stable beyond $\mu = \mu_x$. Fig. 6 shows typical results for $\gamma_p = 10\gamma$, presented as in Fig. 5(a). In this case, different initial conditions as the injection current first crosses the lasing threshold lead to the same qualitative behavior. The initial state of the system just

above threshold is always $\hat{x}$-polarized (labels A and B). As in the previous case, if the injection current is raised enough, this state loses its stability at $\mu = \mu_x$ by way of a supercritical bifurcation to an elliptically polarized state as was true for the conditions of Fig. 5.

When the injection current is increased further, we find a state of mixed polarization (labeled as C) involving periodic modulation of the intensities of the linearly polarized components and a periodic modulation of the total intensity (evident in the equal spacing of the optical sidebands in the field spectra and in the closed curve nature of the n versus N plot). From the various representations and spectra, we infer that this is a state of nearly elliptical polarization with a dominant optical frequency close to that of the horizontally polarized state with about a 1% modulation. The intensity modulation frequency is approximately $20\gamma_p$, which would be the approximate beat frequency between $\hat{x}$-polarized and $\hat{y}$-polarized emissions. This state of time-dependent intensities has a FP value slightly smaller than one indicating that we might think of it as a strong amplitude of an elliptically polarized state at one optical frequency with the addition of two weak fields at different optical frequencies with different polarization states. It appears that this is reached through a supercritical Hopf bifurcation from elliptically polarized steady-state solutions. Thus, it is likely that the additional fields (at different optical frequencies from the main peak) that are evident in the optical spectrum are those represented by the eigenvectors at the Hopf bifurcation point (with specific polarization states and optical frequencies given by positive and negative shifts of the Hopf bifurcation frequency) of the linear stability analysis for the elliptically polarized solutions. While we have only numerical evidence for the six eigenvalues that govern the stability of the elliptically polarized solution, it appears that the boundary denoted by the stars in Fig. 3 is always the result of such a Hopf bifurcation. It is also worth noting that the overall sequence from linear to elliptical to modulated elliptical solutions by way of supercritical steady and Hopf bifurcations, respectively, appears to be common to both of the cases examined in Figs. 5(a) and 6.

For larger injection currents in the conditions of Fig. 6, the system loses almost all of its temporal coherence, presenting broad spectra (probably chaotic, in the sense of deterministic chaos) with a less well-defined principal frequency (state D). The fractional polarization decreases significantly below one as the injection current is increased still further. The time-averaged output powers of the linearly polarized components might be interpreted as "coexistence" of the two linearly polarized modes if one were looking only at the time averaged light–current characteristics for linearly polarized components, but an optical spectral analysis would reveal several sidebands, rather than a single sideband, to the primary spectral peak. Analysis of the polarization states of the spectrally resolved peaks might be required before a decision could be made about the usefulness or validity of a possible interpretation of the result as combination of a few components of definite polarization and different optical frequencies, though the proper basis set for such a description, if it exists, is not the linearly polarized states.

The stability region of elliptically polarized emission (and of the periodically modulated elliptically polarized emission) is very narrow for these parameter values. Hence, elliptically polarized states are not easy to observe in the switching from $\hat{x}$-polarization to the "coexistence" regime. If the model accurately describes the physics, this would indicate that it would also be difficult to observe elliptically polarized solutions in the polarization switching found experimentally.

We finally mention that we have found polarization states that can be characterized by the dynamical coexistence of the two linearly polarized modes with different frequencies. These "two-frequency" solutions appear in the case of very fast mixing of carrier subpopulation between the two channels (large γ_s) such that n is effectively adiabaticaly eliminated in the dynamical evolution. An example of these polarization states is shown in Fig. 7. Just above the lasing threshold, stable simultaneous emission in both $\hat{x}$- and $\hat{y}$-polarizations is observed. Two peaks are observed in the spectrum of the emitted optical field (state labeled α) with nearly equal power in the two spectral components and with the frequency difference corresponding to the birefringence-induced splitting of the linearly polarized single-frequency solutions. The two-frequency state is unstable at currents above $\mu \sim 1.15$. Beyond this current value, only the $\hat{x}$-polarized survives as can be inferred from the field spectrum state (labeled β). The power versus current *(L–I)* characteristic curve shown in this figure has been observed for many circular lasers emitting at room temperature [2], [3]. Qualitatively similar polarization and spectral behavior has been observed for γ_p values in the range $0.5 \leq \gamma_p \leq 20$. All these birefringence values are within the bistability region (region I of Fig. 3) which, for the set of parameters used here, extends up to $\gamma_p/\gamma = 150$ for current values close to threshold. The range of currents for which the two-frequency solutions remain stable is enlarged as the value of spin-flip relaxation rate becomes larger. In the limit of very fast spin-flip mixing ($\gamma_s = \infty$), the population difference n is zero, and two-frequency states are stable for any value of the injection current.

We have limited the studies reported here to values of the injection current for which the experiments indicate that it is reasonable to expect that only the fundamental transverse spatial mode would be lasing. The present version of our model does not account for the appearance of higher order transverse modes as the fields and carrier numbers develop transverse spatial dependence. Transitions to higher order transverse modes are observed experimentally depending on the device parameters, but they usually occur in VCSEL's when the current exceeds between 1.3 and 2 times the threshold current. Then additional polarization switchings are combined with changes in transverse mode profile [1]–[4]. The effects of higher order modes on the polarization state (and spatial mode) selection have been investigated in a suitably modified version of present model [55].

V. ANISOTROPIES IN BOTH AMPLITUDE AND PHASE

In this section, we obtain the steady-state solutions and their stability in the presence of amplitude anisotropy $\gamma_a \neq 0$.
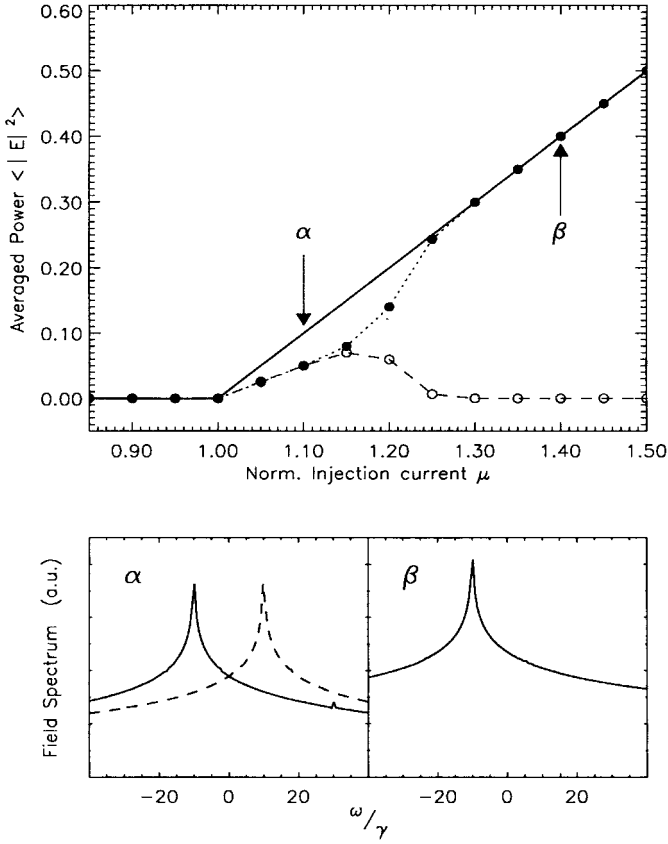
Fig. 7. Two frequency solutions: *L–I* characteristic and optical spectra of the field amplitudes E_x (solid line) and E_y (dashed line) for fast spin-flip relaxation. The parameters used are $\gamma = 1$ ns^{-1}, $\kappa/\gamma = 300$, $\gamma_s/\gamma = 1000$, $\alpha = 3$, $\gamma_p/\gamma = 10.0$.

In this case, the $\hat{x}$- and $\hat{y}$-polarized modes have different thresholds. This is a typical experimental situation as small amplitude anisotropies are unavoidable. We proceed here from the knowledge gained in the simpler case of Section III and follow the same methodology. Assuming a general steady state of the form of (10), we obtain that the $\hat{x}$-polarized solution is given by

$$Q_\pm^2 = \frac{1}{2}\frac{\mu - N_0}{N_0}, \qquad \psi = 0$$
$$\omega_\pm = -\gamma_p + \gamma_a\alpha$$
$$N_0 = 1 + \frac{\gamma_a}{\kappa}, \qquad n_0 = 0 \qquad (41)$$

while the $\hat{y}$-polarized solution is

$$Q_\pm^2 = \frac{1}{2}\frac{\mu - N_0}{N_0}, \qquad \psi = \frac{\pi}{2}$$
$$\omega_\pm = \gamma_p - \gamma_a\alpha$$
$$N_0 = 1 - \frac{\gamma_a}{\kappa}, \qquad n_0 = 0. \qquad (42)$$

These orthogonal linearly polarized solutions have different steady-state amplitudes and different (symmetrically detuned) optical frequencies, though the value of γ_a shifts the frequency splitting from that caused by the birefringence alone ($2\gamma_p$). γ_a (together with α) even creates a splitting of the optical frequencies in the absence of true birefringence, a complication in interpreting experimental lasing spectra for the value of

the birefringence. Moreover, the stability of these solutions is modified by the amplitude anisotropy. Linear stability analysis of (25) for the perturbed solution gives a system of equations for the perturbations which can be decoupled (as for the amplitude isotropic case) into two subsystems for $S = a_+ + a_-$ and $R = a_+ - a_-$. The set of equations for S and Δ is independent of γ_a, so that as in Section III, a given linearly polarized state is stable with respect to perturbations of the field amplitude having the same polarization.

For the stability of a linearly polarized state with respect to perturbations of the field amplitude having the orthogonal polarization, we find

$$\dot{R} = 2\kappa(1 + i\alpha)Q\delta \pm 2(\gamma_a + i\gamma_p)R$$
$$\dot{R}^* = 2\kappa(1 - i\alpha)Q\delta \pm 2(\gamma_a - i\gamma_p)R^*$$
$$\dot{\delta} = -\gamma N_o QR - \gamma N_o QR^* - (\gamma_s + 2\gamma Q^2)\delta \qquad (43)$$

where the lower sign is for the stability of the linearly $\hat{x}$-polarized steady-state solution and the upper sign is for the stability of the linearly $\hat{y}$-polarized steady-state solution. The characteristic polynomial for the eigenvalues λ is

$$P(\lambda) = \lambda^3 + \left(\frac{\gamma_s}{\gamma} + 2Q^2 \mp 4\frac{\gamma_a}{\gamma}\right)\lambda^2$$
$$+ 4\left[\left(\frac{\gamma_p}{\gamma}\right)^2 + \left(\frac{\gamma_a}{\gamma}\right)^2 + \frac{\kappa}{\gamma}Q^2 N_0 \mp \frac{\gamma_a}{\gamma}\left(\frac{\gamma_s}{\gamma} + 2Q^2\right)\right]\lambda$$
$$+ 4\left[\left(\frac{\gamma_p}{\gamma}\right)^2 + \left(\frac{\gamma_a}{\gamma}\right)^2\right]$$
$$\cdot \left(\frac{\gamma_s}{\gamma} + 2Q^2\right) \mp 8\frac{\kappa}{\gamma}Q^2 N_0\left(\frac{\gamma_a}{\gamma} + \alpha\frac{\gamma_p}{\gamma}\right). \qquad (44)$$

The upper and lower signs again correspond to the stability of the $\hat{y}$-polarized and $\hat{x}$-polarized steady-state solutions, respectively, under perturbations of the orthogonal polarization, while N_0 is the steady-state value for the solution [either (41) or (42)] being analyzed for its stability. The amplitude anisotropy breaks the previous symmetry between $\hat{x}$- and $\hat{y}$-polarizations when the sign of the phase anisotropy is changed, as can be inferred from (43). In order to have equivalent stability of the states by interchanging $\hat{x}$ and $\hat{y}$, one has to change both the sign of γ_a and the sign of γ_p. This is consistent with the idea that if we change which polarization state corresponds to a particular optical frequency (which is done by changing the sign of γ_p) we should change the sign of the amplitude anisotropy parameter that prefers one state over the other, if we want to have the modes interchange all of their properties and relative stabilities. For a fixed sign of γ_a, different signs of γ_p correspond to different physical situations because of the fixed sign of the saturable dispersion governed by α.

Proceeding as we did in the case for $\gamma_a = 0$, we can determine the new instability boundaries for the linearly polarized solutions. We have considered two cases in which a small amplitude anisotropy is introduced in the system. The first case is when γ_a is negative (Fig. 8), in which $\hat{x}$-polarized emission is "favored" because its lasing threshold (threshold value of the injection current) is lower than the threshold for
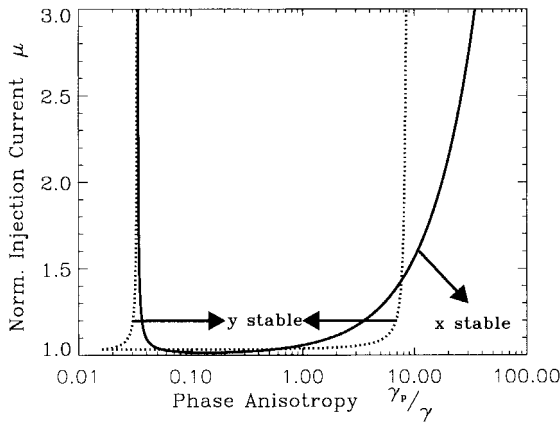
Fig. 8. Stability diagram for $\gamma_a = -0.1\gamma$; other parameters as in Fig. 3. $\hat{x}$-polarized emission has the lower threshold ($\mu = 1 - 1/3000$) and $\hat{x}$-polarized emission is stable below the solid curve. $\hat{y}$-polarized emission is stable between the two dashed curves.
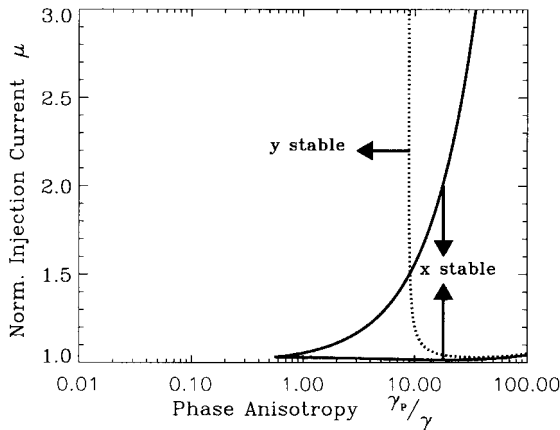

Fig. 9. Stability diagram for $\gamma_a = 0.1\gamma$; other parameters as in Fig. 3. $\hat{y}$-polarization has the lower threshold ($\mu = 1 + 1/3000$) and $\hat{y}$-polarized emission is stable to the left and below the dashed curve. $\hat{x}$-polarized emission is stable between the two solid curves.

existence of the $\hat{y}$-polarized emission. The other situation is when γ_a is positive (Fig. 9), in which the $\hat{y}$-polarization is "favored" because its lasing threshold is lower than that of the $\hat{x}$-polarized state.

In the stability diagram for $\gamma_a = -0.1\gamma$ (shown in Fig. 8), the $\hat{x}$-polarized solution is stable below the solid line, while the $\hat{y}$-polarized solution is stable inside the zone bounded by the dashed curves. There are zones in which only one mode is stable, zones of bistability and zones in which neither linearly polarized mode is stable. As the birefringence (γ_p) goes to zero, only the $\hat{x}$-polarized solution is stable. In a large domain given roughly by $\mu > 1.1$ and $0.03 < \gamma_p/\gamma < 8.0$, only the $\hat{y}$-polarized mode is stable, indicating that despite the favoring by the gain anisotropy for the $\hat{x}$-polarized solution, the emission will switch to $\hat{y}$-polarized emission as the current is increased near threshold, an effect of the combination of saturable dispersion and birefringence similar to that which appeared in Fig. 3. For those values of γ_p for which, as the current is increased the dashed curve is crossed before the solid curve is crossed, there will be hysteresis in the switching points as the injection current is raised from its threshold value where

$\hat{x}$-polarized emission is found (switching at the solid line) or lowered from a value high enough that $\hat{y}$-polarized emission is found initially (switching at the dashed line).

In the stability diagram for $\gamma_a = 0.1\gamma$ (shown in Fig. 9), the $\hat{x}$-polarized solution is stable in the region between the solid curves, while the $\hat{y}$-polarized solution is stable to the left and below the dashed curve. As the birefringence (γ_p) goes to zero, only the $\hat{y}$-polarized solution is stable. For $\gamma_p > 10.0\gamma$ as the current is increased there is a switching of stability from the $\hat{y}$-polarized mode favored near threshold to the $\hat{x}$-polarized mode. Where the dashed curve is above the lower solid curve, there will be hysteresis as the switchings will occur at different values of the current when it is raised or lowered. As in Fig 8, there are also zones of bistability and zones in which neither linearly polarized state is stable.

The main difference in the new values of the parameters from the case of isotropic gain shown in Fig. 3 is that the thresholds for the existence of the two modes differ. For the parameters we have chosen, these differences are small (the threshold current for the favored mode is lowered to $1 - 1/3000$ and the threshold current for the existence of the other mode is raised to $1 + 1/3000$). The somewhat unexpected consequence is that when the injection current is increased, the weaker mode does not always gain stability where the solution exists. Most strikingly, the weak mode does not gain stability for any value of the current when the birefringence is small. These two effects are those which indicate the importance of the gain anisotropy, giving stability only to the mode with the higher gain-to-loss ratio. However, important zones remain near threshold, accessible for typical values of many VCSEL's, in which the saturable dispersion and the birefringence combine to induce switching to the mode with the lower gain-to-loss ratio.

We compare the polarization state switchings observed in these cases with those found in Section IV. If the amplitude anisotropy favors $\hat{y}$-polarized emission as in Fig. 9, the state close to threshold will be always $\hat{y}$-polarized. For $\gamma_p = 2\gamma$ (barring strong noise-induced switching in the bistable region), this polarization state will be retained as the injection current is raised and lowered. However, if the amplitude anisotropy favors $\hat{x}$-polarization as in Fig. 8, the polarized state selected close to threshold will be $\hat{x}$-polarized. In this case, when $\gamma_p = 2\gamma$, we find the same type of switching (from $\hat{x}$-polarized to $\hat{y}$-polarized) when the current is increased, as shown in Fig. 5(a) (recall that what is shown there is one of two possible outcomes depending on the noise-selected initial state at the lasing threshold). Unlike the switching found in the conditions of Fig. 5(a), with the gain anisotropy represented in Fig. 8 there would be a reverse switching from $\hat{y}$-polarized to $\hat{x}$-polarized emission at about $\mu = 1.05$ as the current is lowered (instead of retaining the $\hat{y}$-polarized emission all the way down to the lasing threshold).

The amplitude anisotropy can also force a polarization switching in a situation where it does not exist when $\gamma_a = 0$. As an example, Fig. 10 shows the time-averaged power of each polarized mode for $\gamma_p = 10\gamma$ when $\gamma_a = 0.1\gamma$, where a switching from $\hat{y}$- to $\hat{x}$-polarized emission occurs (compare with Fig. 6). As indicated by the letters on Fig. 10, these
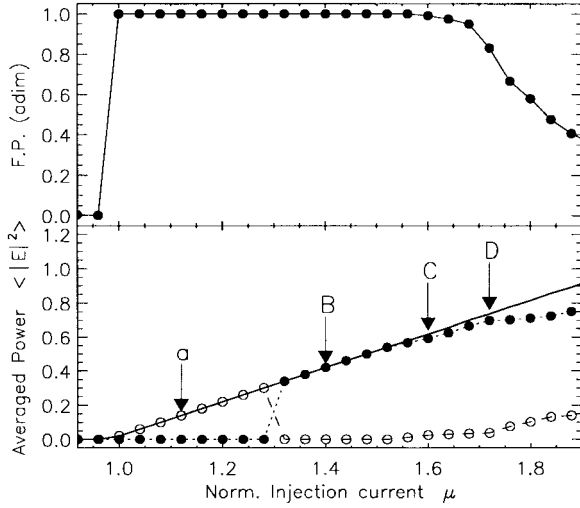
Fig. 10. Light–current characteristic for each linearly polarized mode, and associated fractional polarization for $\gamma_a = 0.1\gamma$. The rest of the parameters are as in Fig. 6.

and other numerical solutions show that zones of elliptically polarized emission, and periodically and chaotically modulated emission, exist in the presence of amplitude anisotropies for values of the current just above some of the instabilitiy boundaries of the linearly polarized solutions where similar states were found in the absence of amplitude anisotropies.

The current at which switching occurs depends on the value of the amplitude anisotropy. For a fixed value of the frequency splitting of the modes, the larger the amplitude anisotropy, the larger the current at which switching occurs. If the amplitude anisotropy is large enough, the $\hat{y}$-polarized state will be the only stable polarization state for all accessible values of the current. If the amplitude anisotropy is small and favors $\hat{x}$-polarized emission, the light–current characteristic is similar to that shown in Fig. 6.

Changes in the amplitude anisotropy are often attributed to thermal effects [3], [13], [46], [56]. Changes in the injection current, lasing power, and number of recombinations change the deposited thermal energy, causing shifts in the cavity frequencies and in the gain profiles. Since the frequency splittings of the cavity modes (γ_p) are very small compared to the width of the gain profile, the gain differences are usually small, though there is a relatively large shift in the wavelengths of emission as the current is varied. These changes in the relative gain for the modes could be modeled in our equations by a dependence on μ of the parameter γ_a or more complex dependences on μ of $\omega_\pm, \gamma_p$, and γ_a.

In this section, we have demonstrated that a combination of birefringence and saturable dispersion can lead to polarization switchings, particularly to the selection (preferential stability) of the mode with lesser gain. This points out that changes in the relative gain that result from heating or from changes in the injection current are not the only factors that influence the stability of linearly polarized solutions when the birefringence and nonlinear dispersion of the semiconductor laser are considered. Which of these is the factor primarily responsible for the experimentally observed switchings may

vary depending on the particular materials. This topic merits detailed experimental study because of the implications for specific designs and applications.

VI. PLANE WAVE VERSUS GAUSSIAN APPROXIMATION

In the previous sections, we neglected the dependence of the laser emission on the transverse coordinates. However, it is known that VCSEL's close to threshold operate with the Gaussian mode TEM$_{00}$. In this section, we show that the linear stability analyses for the plane wave model performed in Sections III and V remain qualitatively valid even if one assumes that the laser beam has a Gaussian transverse profile. We write

$$E_\pm(r,t) = e^{-(r/w_0)^2}e_\pm(t) \tag{45}$$

where w_0 is the beam waist, which can be taken constant along the very short active region in the longitudinal direction. The carrier populations N and n must then be functions of r and t as well. The dynamical equations (2)–(4) become

$$\frac{de_\pm}{dt} = \kappa(1+i\alpha)\left[\int du e^{-u}(N \pm n) - 1\right]e_\pm \\ - i\gamma_p e_\mp - \gamma_a e_\mp \tag{46}$$

$$\frac{\partial N}{\partial t} = -\gamma[N - \mu(u)] - \gamma(N+n)e^{-u}|e_+|^2 \\ - \gamma(N-n)e^{-u}|e_-|^2 \tag{47}$$

$$\frac{\partial n}{\partial t} = -\gamma_s n - \gamma(N+n)e^{-u}|e_+|^2 \\ + \gamma(N-n)e^{-u}|e_-|^2 \tag{48}$$

where we have introduced the new radial variable $u = 2(r/w_0)^2$. We also take the pump parameter μ to be a function of u. If the active region is a cylinder of radius r_A, μ takes two different values for $u < 2(r_A/w_0)^2$ and $u > 2(r_A/w_0)^2$. A finite value of the ratio r_A/w_0 allows us to consider the effects of gain guiding. For simplicity, we assume that the radius of the active region is much larger than the beam waist w_0, so that $2(r_A/w_0)^2 \to \infty$. In this approximation, the pump parameter μ can be taken constant and the integration range for the variable u is $(0, \infty)$.

The linearly $\hat{x}$-polarized state is given by

$$E_\pm = e^{-u/2}Qe^{i(-\gamma_p + \alpha\gamma_a)t} \tag{49}$$

$$1 + \frac{\gamma_a}{\kappa} = \mu\frac{\ln(1+2Q^2)}{2Q^2} \tag{50}$$

and the $\hat{y}$-polarized state by

$$E_\pm = \pm ie^{-u/2}Qe^{i(\gamma_p - \alpha\gamma_a)t} \tag{51}$$

$$1 - \frac{\gamma_a}{\kappa} = \mu\frac{\ln(1+2Q^2)}{2Q^2}. \tag{52}$$

The amplitude Q has been taken real without loss of generality. A comparison with (41) and (42) shows that the thresholds for the two solutions, obtained in the limit $Q \to 0$, coincide with those of the plane wave model ($\mu = 1 \pm \gamma_a/\kappa$). Linear stability analysis yields the following characteristic equation,

where the upper signs hold for the $\hat{x}$-polarized solution and the lower signs hold for the $\hat{y}$-polarized solution:

$$
\left(\lambda + \frac{\gamma_s}{\gamma} - 1\right)\left[\lambda^2 \mp 4\frac{\gamma_a}{\gamma}\lambda + 4\left(\frac{\gamma_p}{\gamma}\right)^2 + 4\left(\frac{\gamma_a}{\gamma}\right)^2\right]
$$
$$
- 2\left(\frac{\kappa}{\gamma} \pm \frac{\gamma_a}{\gamma}\right)\left[\lambda \mp 2\left(\alpha\frac{\gamma_p}{\gamma} + \frac{\gamma_a}{\gamma}\right)\right]
$$
$$
+ 2\left(\lambda + \frac{\gamma_s}{\gamma}\right)\left(\frac{\kappa}{\gamma} \pm \frac{\gamma_a}{\gamma}\right)\left[\lambda \mp 2\left(\frac{\gamma_a}{\gamma} + \alpha\frac{\gamma_p}{\gamma}\right)\right]
$$
$$
\cdot \frac{\ln\left[1 + 2Q^2/(\lambda + \gamma_s/\gamma)\right]}{\ln(1 + 2Q^2)} = 0. \tag{53}
$$

Equation (53) is implicit in λ because λ is contained in the argument of a logarithm. However, we are interested just in finding the stability boundaries, where, by definition, $\mathrm{Re}(\lambda) = 0$. Therefore, we can study (53) in the limit $\mathrm{Re}(\lambda) \ll \gamma_s/\gamma$. Since $\gamma_s \gg \gamma$ and Q^2 is typically of order 1 or less, we can make the following approximation:

$$
\ln\left(1 + \frac{2Q^2}{\lambda + \gamma_s/\gamma}\right) \simeq \frac{2Q^2}{\lambda + \gamma_s/\gamma} = \frac{\mu\kappa}{\kappa \pm \gamma_a}\frac{\ln(1 + 2Q^2)}{\lambda + \gamma_s/\gamma}. \tag{54}
$$

Inserting (54) into (53), we obtain a cubic equation in λ of the form $P(\lambda) = 0$, as in the plane wave case. The characteristic polynomial is

$$
P(\lambda) = \lambda^3 + \left(\frac{\gamma_s}{\gamma} - 1 \mp 4\frac{\gamma_a}{\gamma}\right)\lambda^2
$$
$$
+ 4\left[\left(\frac{\gamma_p}{\gamma}\right)^2 + \left(\frac{\gamma_a}{\gamma}\right)^2 + \frac{\kappa}{\gamma}\frac{\mu - 1}{2}\right.
$$
$$
\left.\mp \frac{\gamma_a}{\gamma}\left(\frac{\gamma_s}{\gamma} - \frac{1}{2}\right)\right]\lambda + 4\left[\left(\frac{\gamma_p}{\gamma}\right)^2 + \left(\frac{\gamma_a}{\gamma}\right)^2\right]
$$
$$
\cdot \left(\frac{\gamma_s}{\gamma} - 1\right) \mp 4\frac{\kappa}{\gamma}\left(\mu - 1 \mp \frac{\gamma_a}{\kappa}\right)\left(\frac{\gamma_a}{\gamma} + \alpha\frac{\gamma_p}{\gamma}\right) \tag{55}
$$

which is very similar to (44). In the limit $\gamma_s \gg \gamma$ and $Q^2 \leq 1$, the two polynomials coincide. For $\gamma_s = 50\gamma$, the stability boundaries defined by (55) are almost indistinguishable from those given by (44) and represented in Fig. 3. We have also checked that the averaged light power versus injected current curve for each polarization state obtained by numerical integration of (46)–(48) coincides with that of Fig. 5(a) if the same parameter values are used (except for a different scaling of average power). This shows that when the transverse profile of the fundamental mode is taken into account, the polarization behavior of the laser is essentially the same as in the plane wave case. More accurate comparisons including gain and index reshaping of the mode are reported in [55].

VII. POLARIZATION SWITCHING INDUCED BY OPTICAL INJECTION

In Sections IV and V, we have shown several examples of polarization switching obtained by varying one of the VCSEL's parameters, namely the pump intensity μ. However, polarization switching can be also obtained by fixing the parameters of the VCSEL and by injecting into the laser an optical signal whose polarization is orthogonal to that emitted by the laser [5], [57]. Two different situations should be considered, depending on the stability of the two linearly polarized states. If the system is bistable, after a sufficiently strong or sufficiently long pulse injected signal causing switching, the laser will remain on the new state. If the system is monostable, the laser will go back to the initial state soon after the injected signal is removed.

We have analyzed both cases, considering the Gaussian model presented in the previous section. The term describing the external field can be easily inserted in the equations. For instance, if one considers injection of a $\hat{y}$-polarized beam, the equations for the field amplitudes are

$$
\frac{de_x}{dt} = \kappa(1 + i\alpha)\left[\int du\, e^{-u}(Ne_x + ine_y) - e_x\right]
$$
$$
- i(\gamma_p + \Delta\omega)e_x - \gamma_a e_x \tag{56}
$$
$$
\frac{de_y}{dt} = \kappa(1 + i\alpha)\left[\int du\, e^{-u}(Ne_y - ine_x) - e_y\right]
$$
$$
+ i(\gamma_p - \Delta\omega)e_y + \gamma_a e_y + \kappa_{\mathrm{inj}}e_{\mathrm{inj}} \tag{57}
$$

where κ_{inj} is the coupling coefficient. (The coupling coefficient coincides with the inverse photon lifetime κ for the ideal case of an effectively mode-matched injected input beam where the injected beam has the same waist as the input beam and does not suffer any misalignment. In addition, one has to assume that the two Bragg reflectors have the same transmissivity to obtain $\kappa_{\mathrm{inj}} = \kappa$.) The amplitude of the injected field is e_{inj} and its frequency ω_{inj} is now taken as the reference frequency. The frequency detuning $\Delta\omega$ is defined as the difference between ω_{inj} and the frequency intermediate between those of the $\hat{x}$-polarized ($\omega_x = -\gamma_p$) and $\hat{y}$-polarized ($\omega_y = \gamma_p$) solutions. Therefore, $\Delta\omega = -\gamma_p$ ($\Delta\omega = \gamma_p$) means that the injected field is resonant with the $\hat{x}$- ($\hat{y}$-) polarized modes of the VCSEL. We have studied the response of the laser to optical injection for different values of the injected power $|e_{\mathrm{inj}}|^2$ and of the frequency detuning $\Delta\omega$, in both bistable and monostable cases.

Fig. 11 presents results for a bistable case corresponding to the parameters of Fig. 3 and $\gamma_p = 2\gamma, \mu = 1.1$ and $\kappa_{\mathrm{inj}} = \kappa$. The frequency detuning $\Delta\omega$ is varied from -6γ to 6γ. For this bistable situation, the injected signal is a rectangular pulse of duration Δt_{inj}. We estimated the injected energy in the following way: the injected power P and the power emitted by the VCSEL P_0 are proportional, respectively, to $|e_{\mathrm{inj}}|^2$ and $2Q^2$, where Q is the stationary amplitude given by (50) and (52). Then the injected energy is

$$
E_{\mathrm{inj}} = P\Delta t_{\mathrm{inj}} = \frac{P}{P_0}P_0\Delta t_{\mathrm{inj}} = \frac{|e_{\mathrm{inj}}|^2}{2Q^2}P_0\Delta t_{\mathrm{inj}}. \tag{58}
$$

We have fixed $\Delta t_{\mathrm{inj}} = 1$ ns in all simulations, and the power P_0 emitted by the VCSEL close to threshold is assumed to be about 0.1 mW. The switching energy is then obtained by inserting in (58) the minimum value of e_{inj} for which switching occurs.

In Fig. 11, the triangles indicate the switching $\hat{y} \to \hat{x}$ by injecting a $\hat{x}$-polarized pulse in a state initially $\hat{y}$-polarized. The circles are for the inverse switching $\hat{x} \to \hat{y}$ caused by
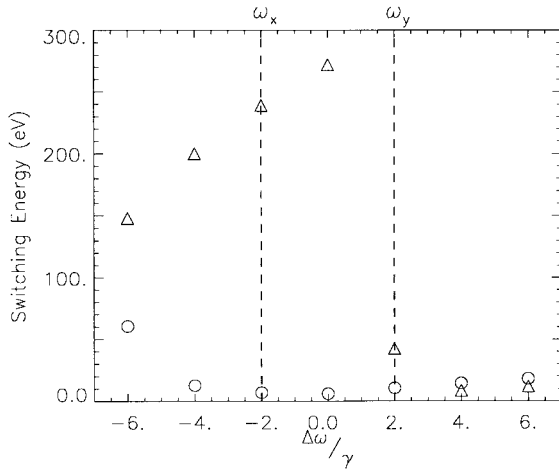
Fig. 11. Switching by injection of 1-ns-long pulses in a bistable situation given by $\mu = 1.1$ from the conditions of Fig. 5 and $\gamma_a = 0.5\gamma$. Switching energy for the transition $\hat{y} \to \hat{x}$ (triangles) and for the opposite transition (circles) as a function of the scaled frequency detuning $\Delta\omega/\gamma$.
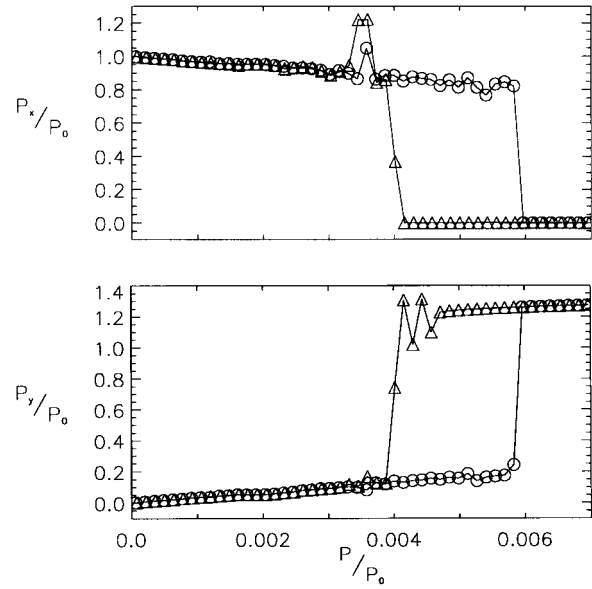

Fig. 12. Switching occurring upon injection of signal with first linearly increasing and then linearly decreasing intensity in a monostable situation. Hysteresis cycles for the power of the $\hat{x}$-polarized and $\hat{y}$-polarized components of the light emitted by the VCSEL versus the normalized injected power. The symbols represent average emitted power over a time interval of 80 ns. The circles refer to the scan with increasing injected power and the triangles to the scan with decreasing injected power. The frequency detuning is $\Delta\omega = -30\gamma$, and $\gamma_a = 0.5\gamma$.

injection of a $\hat{y}$-polarized pulse. The dashed lines indicate resonance of the injected signal with the eventually reached $\hat{x}$- or $\hat{y}$-polarized state. The behavior of the laser is very different for two possible directions of switching. In general, the switching energy is much higher for the first case (switching to the less stable state). It is evident that the most efficient (least energy demanding) switch is accomplished by setting the frequency of the injected signal to a value different from the frequency of the desired final state. This is a reminder that the actual switching transient may be a complicated trajectory in the six-dimensional phase space. For $\Delta\omega/\gamma = 4$ and $\Delta\omega/\gamma = 6$, the switching energies are comparable and very small, on the order of 10 eV. Taking into account that the energy of one photon of wavelength 850 nm is about 1.5 eV, the arrival of 10 photons in 1 ns is enough to make the laser switch in the situation of effectively mode-matched injection considered here.

We next consider a different situation: switching by injection in a parameter region in which there is no bistability. This is the experimental situation described in [5] and we have tried to keep our simulations as close as possible to those experiments. The reported frequency difference between orthogonal linearly polarized emissions is 9 GHz. Taking into account that in our model this frequency difference is given by $2\gamma_p/(2\pi)$, we took $\gamma_p = 30$ rad·ns^{-1}. The amplitude anisotropy parameter γ_a was chosen in such a way that in a scan of the injected current as in Fig. 10, the laser switches from the $\hat{y}$-polarized to the $\hat{x}$-polarized state at about $\mu = 1.2$, in agreement with [5, Fig. 1]. For the other parameters, we used the same values as those used for Fig. 3 and $\kappa_{inj} = \kappa$." We fixed $\mu = 1.5$, above the current at which the polarization switching occurred, where only the $\hat{x}$-polarized state is stable, and we simulated an injected signal of a beam of orthogonally polarized light. Following the experimental procedure, the injected optical power was increased linearly in time until switching occurred, and then the injected power was decreased to zero. In agreement with the experimental results, we found polarization bistability in laser emission, as shown in Fig. 12. Adiabatically sweeping the injected power P from 0% to 0.7% of the emitted power P_0 and back, we found an hysteresis cycle

for both polarization components. Sometimes the switching is not so clean (abrupt) as in Fig. 12, and we have found more gradual transitions from one polarized mode to the other. This feature appears frequently in experimental results. Moreover, in our dynamical simulations, very often the intensities of both modes oscillated, though at high frequencies corresponding to the intermode beatnote frequency $(2\gamma_p)$ and higher harmonics.

The values of power P for which the $\hat{x}$-polarized component of the emitted field switches off and on for different detunings $\Delta\omega$ are shown in Fig. 13. The triangles indicate the switch-off power and the circles indicate the switch-on power. This figure presents many similarities with [5, Fig. 4]. In both cases, the minimum switch-off power is attained when the frequency of the injected field coincides with that of the VCSEL's state with the same polarization (in our case ω_y, in the case of [5] $\omega_\perp$). Moreover, the hysteresis cycle is larger on the small frequency (large wavelength) side, while there is a gradual transition from one polarization to the other on the opposite side. The value of the switching power compared to the power emitted by the VCSEL, which in our results for $\kappa_{inj} = \kappa$ is about three orders of magnitude smaller than in the experiment, depends critically on the value of the coupling parameter κ_{inj}. In the real experiment, most of the injected power is lost because it is very difficult to match perfectly the injected beam and the beam inside the resonator. This leads to a value of κ_{inj} considerably smaller than κ which results in a much larger experimental value of the switching power. In addition, discrepancies between our results and experimental results may also be due to the intensity-induced changes in the frequency differences between the two polarization modes which are not included in our model.
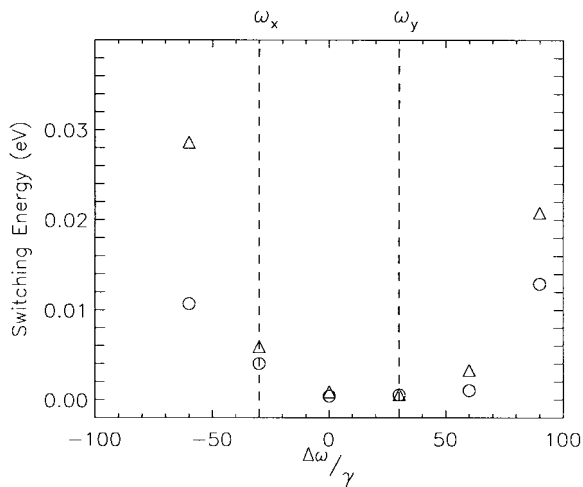
Fig. 13.   Switching points found by injection in a monostable situation as in Fig. 12. Switch-off (triangles) power level for increasing injected power and switch-on (circles) power level for decreasing injected power for different values of the scaled frequency detuning $\Delta\omega/\gamma$.

VIII. CONCLUSION

We have analyzed a rate-equation model that is useful to describe polarization-state selection and polarization-state switchings in VCSEL's operating in the fundamental transverse mode. The model incorporates the effects of birefringence and saturable dispersion as well as gain anisotropies and dynamics of the magnetic sublevel populations. In order to understand the consequences of these ever-present phenomena in semiconductor lasers, we have first discussed in detail the idealized situation of isotropic gain. We then considered more realistic situations in which the effect of saturable dispersion and small gain anisotropies are combined. The effects of the saturable dispersion are often strong enough to preferentially stabilize the linearly polarized mode which has less gain (and a higher threshold current). We have demonstrated polarization switchings as the current is increased that are quite similar to experimental results. We have also demonstrated polarization switchings induced by injected optical fields, including hysteresis, which closely resemble experimental results.

In a small domain of parameters, elliptically polarized states may be found, even in the absence of magnetic fields. We also have provided various views of time-dependent states, including those which are predominantly the superposition of two linearly (or elliptically) polarized fields with different optical frequencies. We have demonstrated the usefulness of a variety of representations of the results (time series, power spectra, polarization-state resolved spectra, Poincaré sphere, fractional polarization, real electric field vector amplitude) which aid in the ultimate interpretation of the observed phenomena.

Extensions of the model presented here should provide additional understanding of VCESL's polarization selection and dynamics and may modify some of our results. Such extensions include the consideration of spatial effects with the emergence of higher transverse modes [55] and the inclusion of current-induced frequency shifts. The effect of magnetic fields on the state selection and the associated dynamics in the context of this model has been discussed elsewhere [48], [58], [59].

Our results suggest that additional insight about VCSEL dynamics may be extracted through careful measurements of the spectra of polarization-state fluctuations and from detailed measurements of the intermediate states in the polarization-state switchings which are observed. Careful determination, for example, of the hysteresis, if any, in the current-induced polarization switchings would also be useful for determining the appropriate values of the parameters to use in modeling this behavior.

REFERENCES

[1] C. J. Chang-Hasnain, J. P. Harbison, G. Hasnain, A. C. Von Lehmen, L. T. Florez and N. G. Stoffel, "Dynamics, polarization, and transverse mode characteristics of vertical-cavity surface-emitting lasers," *IEEE J. Quantum Electron.*, vol. 27, pp. 1402–1409, 1991.
[2] K. D. Choquette and R. E. Leibenguth, "Control of vertical-cavity laser polarization with anisotropic transverse cavity geometries," *IEEE Photon. Technol. Lett.*, vol. 6, pp. 40–42, 1994.
[3] K. D. Choquette, D. A. Richie, and R. E. Leibenguth, "Temperature dependence of gain-guided vertical-cavity surface emitting laser polarization," *Appl. Phys. Lett.*, vol. 64, no. 16, pp. 2062–2064, 1994.
[4] H. Li, T. L. Lucas, J. G. McInerney, and R. A. Morgan, "Transverse modes and patterns of electrically pumped vertical-cavity surface-emitting semiconductor lasers," *Chaos, Solitons and Fractals*, vol. 4, pp. 1619–1636, 1994.
[5] Z. G. Pan, S. Jiang, M. Dagenais, R. A. Morgan, K. Hojima, M. T. Asom, and R. E. Leibenguth, "Optical injection induced polarization bistability in vertical-cavity surface-emitting lasers," *Appl. Phys. Lett.*, vol. 63, no. 22, pp. 2999–3001, 1993.
[6] A. Chavez-Pirson, H. Ando, H. Saito, and H. Kanbe, "Polarization properties of a vertical-cavity surface emitting laser using a fractional layer superlattice gain medium," *Appl. Phys. Lett.*, vol. 62, no. 24, pp. 3082–3084, 1993.
[7] K. D. Choquette, K. L. Lear, R. E. Leibenguth, and M. T. Asom, "Polarization modulation of cruciform vertical-cavity laser diodes," *Appl. Phys. Lett.*, vol. 64, no. 21, pp. 2767–2769, 1994.
[8] A. K. Jansen van Doorn, M. P. van Exter, and J. P. Woerdman, "Effects of transverse anisotropy on VCSEL spectra," *Electron. Lett.*, vol. 30, no. 23, pp. 1941–1943, 1994.
[9] S. Jiang, Z. Pan, M. Dagenais, R. A. Morgan, and K. Kojima, "High-frequency polarization self-modulation in vertical-cavity surface-emitting lasers," *Appl. Phys. Lett.*, vol. 63, no. 26, pp. 3545–3547, 1993.
[10] K. D. Choquette, R. P. Schneider, Jr., K. L. Lear, and R. E. Leibenguth, "Gain-dependent polarization properties of Vertical-Cavity lasers," *IEEE J. Select. Topics Quantum Electron.*, vol. 1, pp. 661–666, 1995
[11] A. K. Jansen van Doorn, M. P. van Exter, and J. P. Woerdman, "Tailoring the birefringence in a vertical-cavity semiconductor laser," *Appl. Phys. Lett.*, vol. 69, no. 24, pp. 3635–3537, 1996.
[12] C. J. Chang-Hasnain, J. P. Harbison, L. T. Florez, and N. G. Stoffel, "Polarization characteristics of quantum-well vertical-cavity surface-emitting lasers," *Electron. Lett.*, vol. 27, no. 1, pp. 163–165, 1991.
[13] G. Hasnain, K. Tai, L. Yang, Y. H. Wang, R. J. Fischer, J. D. Wynn, B. Weir, N. K. Dutta, and A. Y. Cho, "Performance of gain-guided surface emitting lasers with semiconductor distributed Bragg reflectors," *IEEE J. Quantum Electron.*, vol. 27, pp. 1377–1385, 1991.
[14] H. Kobayashi, H. Iwamura, T. Saku, and K. Otsuka, "Polarization-dependent gain-current relationship in GaAs-AlGaAs MQW laser diodes," *Electron. Lett.*, vol. 19, no. 5, pp. 166–168, 1983.
[15] J. Martin-Regalado, M. San Miguel, N. B. Abraham, and F. Prati, "Polarization switching in quantum well vertical-cavity surface emitting lasers," *Opt. Lett.*, vol. 21, no. 5, pp. 351–353, 1996.
[16] _____, "Polarization state selection and switching in VCSELs," in *Physics and Simulation of Optoelectronic Devices IV*, W. W. Chow and M. Osinski, Eds. Bellingham, WA: SPIE, 1996, vol. 2693, pp. 213–220.
[17] H. Haug and H. Haken, "Theory of noise in semiconductor laser emission," *Z. Phys.*, vol. 204, pp. 262–274, 1967.
[18] C. H. Henry, "Theory of the linewidth enhancement factor of semiconductor lasers," *IEEE J. Quantum Electron.*, vol. QE-18, pp. 259–264, 1982.
[19] M. Osinski and J. Buus, "Linewidth broadening factor in semiconductor lasers—An overview," *IEEE J. Quantum Electron.*, vol. QE-23, pp. 9–29, 1987.

[20] W. van Haeringen, "Polarization properties of a single-mode operating gas laser in a small axial magnetic field," *Phys. Rev.*, vol. 158, no. 2, pp. 256–272, 1967.

[21] W. J. Tomlinson and R. L. Fork, "Properties of gaseous optical masers in weak axial magnetic fields," *Phys. Rev.*, vol. 164, no. 2, pp. 466–483, 1967.

[22] H. de Lang, D. Polder, and W. van Haeringen, "Optical polarization effects in a gas laser," *Phillips Tech. Rev.*, vol. 32, pp. 190–204, 1971.

[23] D. Lenstra, "On the theory of polarization effects in gas lasers," *Phys. Reps.*, vol. 59, no. 3, pp. 299–373, 1980.

[24] D. Polder and W. van Haeringen, "Circular polarization in a $j = 1 \rightarrow j = 0$ transition laser," *Phys. Lett.*, vol. 25A, no. 4, pp. 337–338, 1967.

[25] G. Bowhuis, "On the anomalous circular polarization of the 1.523 μ HeNe laser line," *Phys. Lett.*, vol. 27A, no. 10, pp. 693, 1968.

[26] W. van Haeringen and H. de Lang, "Role of linear phase anisotropy in a Zeeman laser," *Phys. Rev.*, vol. 180, no. 2, pp. 624–625, 1969.

[27] R. L. Fork and M. Sargent, III, "Mode competition and frequency splitting in magnetic field-tuned optical masers," *Phys. Rev.*, vol. 139, no. 3A, pp. 617–618, 1965.

[28] M. Sargent, III, W. E. Lamb, Jr., and R. L. Fork, "Theory of a Zeeman laser I," *Phys. Rev.*, vol. 164, no. 2, pp. 436–449, 1967.

[29] M. Matlin, R. Gioggia, N. B. Abraham, P. Glorieux, and T. Crawford, "Polarization switch in a Zeeman laser in the presence of dynamical instabilities," *Opt. Commun.*, vol. 120, pp. 204–222, 1995.

[30] A. D. May, P. Paddon, E. Sjerve, and G. Stephan, "An alternative interpretation of the Zeeman and Faraday laser," *Phys. Rev. A*, vol. 53, no. 4, pp. 2829–2841, 1996.

[31] N. B. Abraham, E. Arimondo, and M. San Miguel, "Polarization state selection and stability in a laser with a polarization isotropic resonator: An example of no lasing despite inversion above threshold," *Opt. Commun.*, vol. 117, pp. 344–356, 1995; erratum: vol. 1, p. 168, 1995.

[32] M. San Miguel, Q. Feng, and J. V. Moloney, "Light-polarization dynamics in surface-emitting semiconductor lasers," *Phys. Rev. A*, vol. 52, no. 2, pp. 1728–1739, 1995.

[33] W. W. Chow, S. W. Koch, and M. Sargent III, *Semiconductor-Laser Physics*. Berlin, Germany: Springer-Verlag, 1994, ch. 6.

[34] F. Meier and B. P. Zachachrenya, Eds., *Optical Orientation*. Amsterdam, The Netherlands: North Holland, 1984.

[35] T. Uenoyama and L. J. Sham, "Carrier relaxation and luminiscence polarization in quantum wells," *Phys. Rev. B*, vol. 42, no. 11, pp. 7114–7123, 1990.

[36] T. C. Damen, L. Vina, J. E. Cunningham, J. Shah, and L. J. Sham, "Subpicosecond spin relaxation dynamics of excitons and free carriers in GaAs quantum wells," *Phys. Rev. Lett.*, vol. 67, no. 24, pp. 3432–3435, 1991.

[37] S. Bar-Ad and I. Bar-Joseph, "Exciton spin dynamics in GaAs heterostructures," *Phys. Rev. Lett.*, vol. 68, no. 3, pp. 349–352, 1992.

[38] I. Muñoz, E. Pérez, V. Bellani, S. Zimmermann, L. Viña, K. Ploog, E. S. Koteles, and K. M. Lau, "Exciton dynamics and spin relaxation in unstrained and tensile-strained quantum wells," *J. Opt. Soc. Amer. B*, vol. 13, no. 5, pp. 994–999, 1996.

[39] R. Ferreira and G. Bastard, "Spin-flip scattering of holes in semiconductor quantum wells," *Phys. Rev. B*, vol. 43, no. 12, pp. 9687–9691, 1991.

[40] V. Srinivas, Y. J. Chen, and C. E. C. Wood, "Intrinsic and extrinsic processes in photoluminiscence, reflectivity, and spin dynamics of GaAs quantum wells," *J. Opt. Soc. Amer. B*, vol. 13, no. 5, pp. 989–993, 1996.

[41] M. Z. Maialle, E. A de Andrada e Silva, and L. J. Sham, "Exciton spin dynamics in quantum wells," *Phys. Rev. B*, vol. 47, no. 23, pp. 15776–15788, 1993.

[42] D. Robart, T. Amand, X. Marie, M. Brousseau, J. Barrau, and G. Bacquet, "Exciton-exciton interaction under elliptically polarized light excitation," *J. Opt. Soc. Amer. B*, vol. 13, no. 5, pp. 1000–1008, 1996.

[43] J. W. Scott, B. J. Thibeault, C. J. Mahon, L. A. Coldren, and F. H. Petters, "High modulation efficiency of intracavity contacted vertical cavity lasers," *Appl. Phys. Lett.*, vol. 65, no. 12, pp. 1483–1485, 1994.

[44] D. Tauber, G. Wang, R. S. Geels, J. C. Bowers, and L. A. Coldren, "Large and small signal dynamics of vertical-cavity surface-emitting lasers," *Appl. Phys. Lett.*, vol. 62, no. 4, pp. 325–327, 1993.

[45] T. Ohtoshi, T. Kuroda, A. Niwa, and S. Tsuji, "Dependence of optical gain on crystal orientation in surface-emitting lasers with strained quantum wells," *Appl. Phys. Lett.*, vol. 65, no. 15, pp. 1886–1887, 1994.

[46] J. P. Zhang, "The dynamic properties and stability analysis for vertical-cavity surface-emitting lasers," *IEEE J. Quantum Electron.*, vol. 31, pp. 2127–2132, 1995.

[47] T. Mukaihara, F. Koyama, and K. Iga, "Engineered polarization control of GaAs/AlGaAs surface-emitting lasers by anisotropic stress from elliptical etched substrate hole," *IEEE Photon. Technol. Lett.*, vol. 5, pp. 133–135, 1993.

[48] A. K. Jansen van Doorn, M. P. van Exter, M. Travagnin, and J. P. Woerdman, "Polarization behavior of surface-emitting semiconductor lasers in an axial magnetic field," *Opt. Commun.*, vol. 133, nos. 1–6, 252–258, 1997.

[49] M. P. van Exter, A. K. Jansen van Doorn, and J. P. Woerdman, "Transverse anisotropy and mode structure in VCSELs," in *Physics and Simulation of Optoelectronic Devices IV*, W.W. Chow and M. Osinski, Eds. Bellingham, WA: SPIE, 1996, vol. 2693, pp. 202–212.

[50] T. B. Simpson and J. M. Liu, "Spontaneous emission, nonlinear optical coupling, and noise in laser diodes," *Opt. Commun.*, vol. 112, no. 1, pp. 43–47, 1994.

[51] P. Mandel and T. Erneux, "Laser Lorenz equations with a time-dependent parameter," *Phys. Rev. Lett.*, vol. 53, pp. 1818-1821, 1984.

[52] P. Mandel, "Dynamic versus static stability," in *Frontiers in Quantum Optics*, E. R. Pike and S. Sarkar, Eds. Boston, MA: Adam Hilger, 1986.

[53] P. Mandel, "Birfurcation problems in nonlinear optics," in *Instabilities and Chaos in Quantum Optics II*, N. B. Abraham, F. T. Arecchi, and L. A. Lugiato, Eds. New York: Plenum, 1988, pp. 321–334.

[54] J. M. Stone, *Radiation and Optics*. New York: McGraw-Hill, 1963.

[55] J. Martin-Regalado, S. Balle, M. San Miguel, "Polarization and transverse mode dynamics of gain-guided vertical cavity surface emitting lasers," *Opt. Lett.*, vol. 27, no. 4, April 1997.

[56] H. Kawaguchi, I. S. Hidayat, Y. Takahashi, and Y. Yamayoshi, "Pitch-fork bifurcation polarization bistability in vertical-cavity surface emitting lasers," *Electron. Lett.*, vol. 31, no. 2, pp. 109–110, 1995.

[57] G. R. Hadley, K. L. Lear, M. E. Warren, K. D. Choquette, J. W. Scott, and S. W. Corzine, "Comprehensive numerical modeling of vertical-cavity surface-emitting lasers," *IEEE J. Quantum Electron.*, vol. 32, pp. 607–616, 1996.

[58] C. Serrat, N. B. Abraham, M. San Miguel, R. Vilaseca, and J. Martin-Regalado, "Polarization dynamics in a vertical cavity laser with an axial magnetic field," *Phys. Rev. A*, vol. 53, no. 6, pp. R3731–R3733, 1996.

[59] M. Travagnin, M. P. van Exter, A. K. Jansen van Doorn, and J. P. Woerdman, "Role of optical anisotropies in the polarization properties of surface-emitting semiconductor lasers," *Phys. Rev. A*, vol. 54, no. 2, 1647–1660, 1996.

J. Martin-Regalado, photograph and biography not available at the time of publication.

F. Prati, photograph and biography not available at the time of publication.

M. San Miguel, photograph and biography not available at the time of publication.

N. B. Abraham (M'94), photograph and biography not available at the time of publication.